Molecular Docking and Dynamics Identify Potential Drugs to be Repurposed as SARS-CoV-2 Inhibitors

Mohammed Muzaffar-Ur-Rehman, Chougule Kishore Suryakant, Ala Chandu, Banoth Karan Kumar, Renuka Parshuram Joshi, Snehal Rajkumar Jadav, Murugesan Sankaranarayanan, Seshadri S Vasan

Journal of Computational Biophysics and Chemistry

World Scientific
www.worldscientific.com

Molecular docking and dynamics identify potential drugs to be repurposed as SARS-CoV-2 inhibitors

Mohammed Muzaffar-Ur-Rehman

Department of Pharmacy, Birla Institute of Technology and Science
Pilani, Rajasthan 333031, India[*]
p20210457@pilani.bits.pilani.ac.in

Chougule Kishor Suryakant

Department of Pharmacy, Birla Institute of Technology and Science
Pilani, Rajasthan 333031, India
h20210293@pilani.bits.pilani.ac.in

Ala Chandu

Department of Pharmacy, Birla Institute of Technology and Science
Pilani, Rajasthan 333031, India
p20210055@pilani.bits.pilani.ac.in

Banoth Karan Kumar

Department of Pharmacy, Birla Institute of Technology and Science
Pilani, Rajasthan 333031, India
Karanbanith@gmail.com

Renuka Parshuram Joshi

Department of Pharmacy, Birla Institute of Technology and Science
Pilani, Rajasthan 333031, India
h20210291@pilani.bits.pilani.ac.in

Snehal Rajkumar Jadav

Department of Pharmacy, Birla Institute of Technology and Science
Pilani, Rajasthan 333031, India
h20210289@pilani.bits.pilani.ac.in

Murugesan Sankaranarayanan[†]

Department of Pharmacy, Birla Institute of Technology and Science
Pilani, Rajasthan 333031, India
murugesan@pilani.bits-pilani.ac.in

[*]State completely without abbreviations, the affiliation and mailing address, including country typeset in 8 pt times italic.
[†]Typeset names in 8 pt Times Roman. Use the footnote to indicate the present or permanent address of the author.

Seshadri S Vasan

School of Medical and Health Sciences, Edith Cowan University
Joondalup, WA 6027, Australia.
Department of Health Sciences, University of York
York YO10 5DD, United Kingdom.
prof.vasan@york.ac.uk

Received (Day Month Year)
Revised (Day Month Year)
Accepted (Day Month Year)

The novel coronavirus disease 19 (COVID-19) has resulted in an estimated 20 million excess deaths and the recent resurgence of COVID-19 in China is predicted to result in up to 1 million deaths over the next few months. With vaccines being ineffective in the case of immune-compromised patients, it is important to continue our quest for safe, effective, affordable drugs that will be available to all countries. Drug repurposing is one of the strategies being explored in this context. Recently, out of 7,817 drugs approved worldwide, 214 candidates were systematically down-selected using a combination of 11 filters including FDA/TGA approval status, assay data against SARS-CoV-2, pharmacokinetic, pharmacodynamic and toxicity profiles. These down-selected drugs were subjected in this study to virtual screening against various SARS-CoV-2 targets followed by molecular dynamic studies of the best scoring ligands against each target. The chosen molecular targets were Spike receptor binding domain, Nucleocapsid protein RNA binding domain, and key non-structural proteins 3, 5, 12, 13 and 14. Four drugs approved for other indications — alendronate, cromolyn, natamycin and treprostinil — look sufficiently promising from our *in-silico* studies to warrant further in vitro and in vivo investigations as appropriate to ascertain their extent of antiviral activities.

Keywords: COVID-19; drug repurposing; long COVID; molecular docking; molecular dynamics; SARS-CoV-2.

1. Introduction

The novel coronavirus disease 19 (COVID-19) and the post COVID-19 condition called long COVID have affected lives and livelihoods across the world. As of 20 April 2023, we had over 685 million confirmed COVID-19 cases and 6.8 million deaths recorded globally [1] and an estimated 20 million excess deaths obtained by extrapolating the findings published recently in *The Lancet* [2]. According to the WHO, circa 144 million people suffered from long COVID by the end of 2021 when the recorded cases stood at around 278 million [3,4], therefore we are likely to have circa 355 million long COVID patients worldwide already. The recent resurgence of COVID-19 in China is predicted to result in up to 1 million deaths over the next few months [5.]

COVID-19 is caused by the severe acute respiratory syndrome coronavirus 2 (SARS-CoV-2), which is part of the RNA virus family. It possesses four structural proteins (S, E, M, and N as defined below) and sixteen non-structural proteins (NSP1−16) [6]. The capsid formed from the nucleocapsid protein (N) is present outside the positive-sense, single-stranded RNA genome (+ssRNA) and the genome is further covered by an envelope that is mainly related to three structural proteins: membrane protein (M), spike protein (S), and envelope protein (E). Spike glycoproteins (S protein) form homotrimers that protrude from the host-derived viral envelope and furnish specificity for cellular entry receptors [7]. The non-structural proteins (NSP's) have vital role in the viral replication, and repair. For instance, NSP3 (papain like protease) and NSP5 (main protease) are involved cleaving the polypeptide chains to produce other subunits (NSPs1-16). Among these, NSP3, 4 and 6 forms a replication/transcription complex (RTC) that helps in replication and transcription process. NSP12,7 and 8 are required for the production of viral RNA and maintain its stability [8]. Other nonstructural proteins such as NSP13 (helicase) is necessary for the viral replication, recombination and repair [9,10]; and NSP14 (exoribonuclease domain) is required for proof reading mechanism during viral synthesis [11,12]. Therefore, targeting these proteins using certain inhibitors, will have a major impact on the virus' structural integrity, thereby achieving antiviral function.

Vaccines have been useful to restore a level of normalcy but its efficiency in immunocompromised patients are low as they did not respond well to the vaccines [13,14] which leaves at a greater risk of COVID-19 associated mortality [15]. A study conducted by Wallace *et al.,* in 2021 reveals ~3% of the current population (336.6 million) is immunosuppressed which accounts for >10 million people in United states alone [16]. The numbers of immunosuppressed patients are several folds higher when the entire population across the globe is considered. Additionally, most part of the population suffering from autoimmune disorders such as graves' disease, rheumatoid arthritis, vitiligo, diabetes mellitus, etc., have been using immunosuppressive agents leaving them more prone to other infections especially viral [17,18]. Therefore, to address the need for these patients, it is important to develop affordable therapies that are safe, effective and available, especially to low- and lower-middle income countries.

Various antiviral drugs had been developed such as remdesivir, molnupiravir, favipiravir, nirmatrelvir, etc. but none of these meet all four requirements mentioned above. Remdesivir is a prodrug is available as a parenteral [19], while molnupiravir was not shown to have a good clinical outcome from the clinical trials data [20,21]. Favipiravir was found to be not effective against disease progression [22] and nirmatrelvir, a medication developed by Pfizer is very potent in combination with ritonavir, but has a high price and low manufacturing capability to cater to global demand [23,24]. Several *in silico* reports are also available wherein the libraries of molecules were virtually screened to get hits against SARS-CoV-2 targets, but the safety parameter was not considered as their results include drugs with adverse effects [25–31].

Unfortunately, the investment required to get a new drug to market is very high; for example, the mean and median capitalized research and development investment of getting a new drug to market were US$1335.9 million and US$985.3 million respectively,

for the period 2008-19 [32], therefore repurposing drugs approved for other indications to combat COVID-19 and long COVID is a worthwhile strategy [33]. This approach looks for new uses for approved or investigational drugs that are outside the scope of the original medical indication, and can dramatically shrink the costs and timeline involved. However, a major challenge is that there are 7,817 candidates in the *Compounds Australia* open drug collection, so we recently developed a database to down-select the top candidates in a systematic manner [34,35]. To validate our approach experimentally, 12 of the top 214 drugs, along with the current standards of care (remdesivir, molnupiravir and nirmatrelvir/ritonavir), were recently subjected to *in vitro* evaluation of antiviral efficacy against SARS-CoV-2 Delta and Omicron variants of concern [36]. To decide which additional candidates from the list of 214 drugs should be evaluated next, this study reports an *in silico* evaluation of diverse range of drugs against SARS-CoV-2 targets by utilizing molecular docking, MM-GBSA and molecular dynamics simulation studies. These tools enable the prediction of drug-viral target binding interactions, aiding in the selection of drugs with higher likelihoods of success. It also expands our understanding of potential treatments and optimizes the drug discovery process, making significant strides in advancing the current knowledge of COVID-19 therapeutics.

2. Materials and Methods

Jain *et al.* [34] have developed the open access, user-friendly 'CoviRx' platform to display each of these 7,817 drugs, along with their physical and chemical properties, original indication, available data from multiple assays, COVID-19 clinical trials, any red flags such as pregnancy concerns, contraindications, etc. and drugs that are similar to the query on the basis of the Tanimoto coefficient [37]. This work made use of CoviRx.org along with the pharmacological down-selection methodology described by MacRaild *et al.* [35] involving a combination of filters such as approval status, assay data against SARS-CoV-2, pharmacokinetic, pharmacodynamic and toxicity profiles. In addition, the pregnancy and pan-assay interference compounds (PAINS) categories were included to rule out drugs unsafe for pregnant women and those likely to produce false positive results (Figure 1). In this study, the 214 drugs which passed all the filters were subjected to molecular docking studies against various targets of SARS-CoV-2 followed by molecular dynamic simulations of the best scoring ligands against each target (work flow depicted in Figure 1) [38]. The molecular targets include spike receptor binding domain (RBD), nucleocapsid protein RNA binding domain (NPRBD), and selected non-structural proteins (NSPs) such as RNA-dependent RNA polymerase (RdRp), papain-like protease (PL pro), 3-Chymotrypsin Like protease/main protease (3CL pro/ M pro), helicase, and exoribonuclease domain (Table 1) [7].

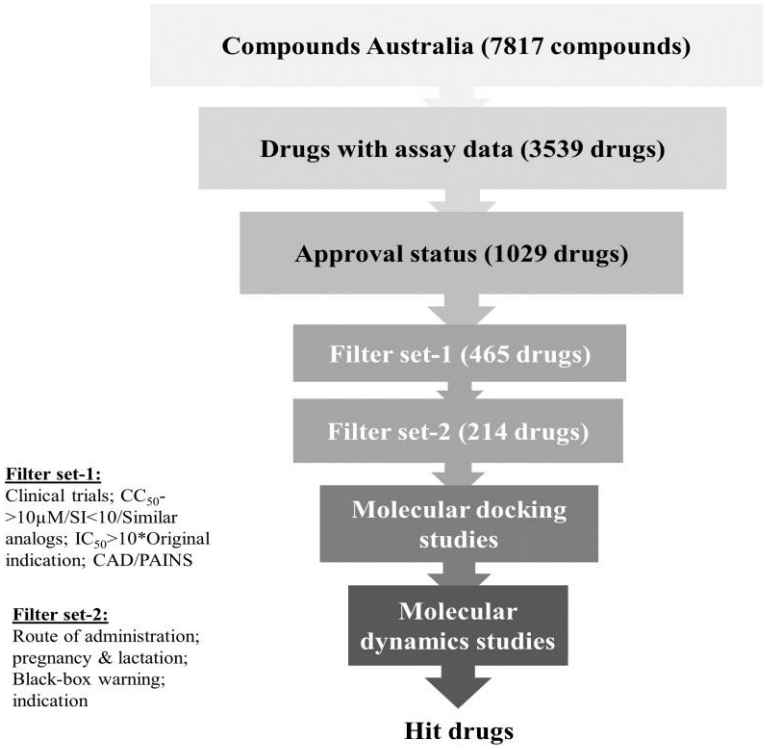

Figure 1. Workflow of the shortlisting methodology used for down-selection and their molecular docking and dynamics studies

2.1. Protein preparation

The virus-based targets with good resolution were downloaded from the protein data bank (PDB) (https://www.rcsb.org/). These proteins were prepared by adding hydrogens, refining the protein by optimization using the module PROPKA at pH 7.0, by removing water molecules beyond 3.0 Å, followed by structural minimization. PROPKA predicts the pKa values of ionizable groups in proteins and protein-ligand complexes based on the 3D structure. This process was performed using the protein preparation wizard of Maestro 22 (Schrodinger, LLC, New York, NY, 2022) [39]. The details of virus-based protein targets used in the current study and their respective PDB IDs are shown in Table 1.

Table 1. Targets used for virtual screening

S. No	Target protein	PDB ID	Resolution
1.	Spike receptor binding domain	6M0J	2.45 Å
2.	Nucleocapsid protein RNA binding domain	6VYO	2.2 Å
3.	Papain Like protease (NSP3)	6W9C	2.7 Å
4.	Main protease (3CL protease) (NSP5)	6W63	2.1 Å
5.	RNA dependent RNA polymerase (NSP12)	6M71	2.9 Å
6.	Helicase (NSP13)	7NNG	2.38 Å
7.	Exoribonuclease domain (NSP14)	7R2V	2.53 Å

2.2. Ligand preparation

The short-listed drugs (214) were downloaded from PubChem database in "sdf" format (https://pubchem.ncbi.nlm.nih.gov/). These drugs's 2D structures were imported in the Maestro, and the LigPrep module was used to prepare the ligands by applying optimize potentials for liquid simulation (OPLS4) force field. During the ligand preparation process, ionization was set to neutralize using the Epik module of Schrodinger suite. The chirality of

the structures were determined from their 3D structures. The obtained minimized structures were used further to carry out molecular docking studies.

2.3. Grid generation

Receptor grid generation wizard was used to select the native position of the co-crystal ligands to validate the docking protocol. If a protein did not possess co-crystal ligand, then an extensive literature search was conducted to look for the x, y and z co-ordinates to be given as input to the grid wizard (Table 2). On the other hand, for the spike protein (6M0J), as it does not possess a co-crystal ligand, the key interacting residues with the Angiotensin converting enzyme 2 (ACE2) were considered as the center of the grid.

Table 2: Grid co-ordinates of proteins with no co-crystal ligand

S. No	PDB ID	X-axis	Y-axis	Z-axis
1.	6M71 [40]	120.535	116.572	140.185
2.	6W9C [41]	-46.0103	14.2997	29.9464
3.	6VYO [42]	-19.843	10.273	-6.002

2.4. Molecular docking and MM-GBSA studies

The ligands prepared using ligprep module, the minimized protein and the generated grid files were used for performing flexible ligand docking studies in extra precision (XP) mode by adding Epik state penalties. The docking study was carried out in the glide module (Maestro, v13.3; Schrodinger LLC). The number of poses to be included were set to ten and the best pose among them is reported in this study. All other default parameters were retained. Molecular Mechanics-Generalized Born Surface Area (MM-GBSA) is a computational method used to estimate the binding free energy between the bound state and the unbound state of a bio-molecular complex. The change in energy upon complex formation (ΔE_{MM}) is summed up with the change in free energy of the solvation (ΔG_{solv}) and the surface area (ΔG_{SA}). For the free energy calculations (MM-GBSA) via prime module, the docked complexes of the top scoring drugs were used and solvation model was variable-dielectric generalized born model (VSGB) in the presence of OPLS4 force field [43]. Following formula is utilized for calculating the ΔG_{bind} of the selected ligands.

$$\Delta G_{bind} = \Delta E_{MM} + \Delta G_{solv} + \Delta G_{SA}$$

2.5. Molecular dynamics (MD) studies

The workstation used to perform the dynamics studies was of Tyrone, equipped with 120GB HDD and 12GB of NVIDIA graphic card. The solvent model used was of transferable intermolecular potential 3P (TIP3P) and the temperature was set to 310.15K. Firstly, the protein was preprocessed to identify the problems if any, and rectified by adding hydrogens and filling the missing residues using prime module of the software. Further, water molecules beyond 5 Å were removed and at pH of 7.0 ± 2.0, heteroatoms state was generated using the software's Epik module [44]. Secondly, system builder wizard of Desmond module (Schrodinger, LLC) was run by choosing the TIP3P solvent model using OPLS4 force filed and generating an orthorhombic box with dimensions of 10x10x10 Å [45,46]. The number of ions required to neutralize the system was calculated and added. In addition, salt with concentration of 0.15 M was checked in. Thirdly, the output of system builder was used to carry out minimization step for the entire system of complex and solvent for 100ps. Lastly, MD simulation was run using isothermal-isobaric ensemble with constant number of particles (NPT) mode for 100ns.

3. Results and Discussion

3.1. Docking validation

To validate the protein-ligand interaction, the co-crystal ligands from the respective targets were extracted and re-docked in the same grid as that of the native ligand [47]. Among nine, only three targets (NSP5 (3CL pro), NSP13 (helicase), and NSP14 (exoribonuclease domain)) possess the co-crystalized ligands, therefore validation was carried to these three. Among these, for the protein corresponding to 3CL protease (PDB: 6W63) the random mean square deviation (RMSD) score of the co-crystal ligand was 1.6984 Å. For NSP13 (PDB: 7NNG) and NSP14 (PDB: 7R2V), the RMSD for corresponding co-crystals were 0.3814 Å and 1.035 Å, respectively. As the RMSD was <2 Å, the docking methodology followed is within the acceptable limit and can be used further for docking the ligands (Figure 2).

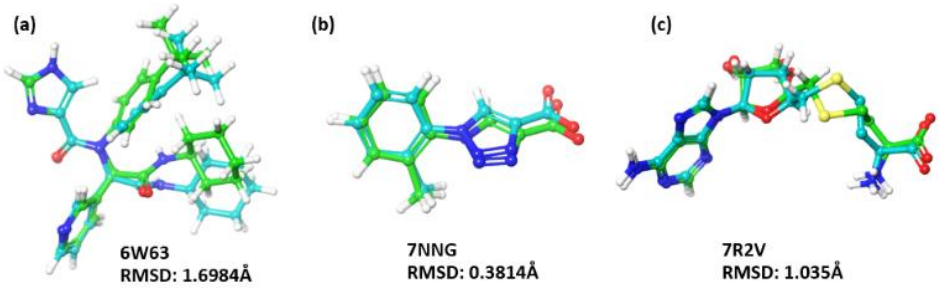

Figure 2. Co-crystal RMSD of (a) 3CL protease (b) Helicase (c) Exoribonuclease domain; green color represents native ligand and blue represents redocked pose

3.2. Screening of drugs and MD studies

The shortlisted drugs among the FDA/TGA approved were subjected to docking studies against seven different virus-based targets. Few molecules that failed to bind to the targets in the docking studies were excluded. From this screening process, the drug with the least binding energy against each target was subjected to MM-GBSA studies followed by MD studies. The overall summary of the docking scores are represented as graph in Figure 3; the docking score of each drugs with all the targets are tabulated in the supplementary file **(S1),** the docking results corresponding to top drugs against each target along with their free energy scores were shown in Table 3, 4, and Figure 4, and the original indication details of the hit durgs were shown in Table 5. Results of molecular dynamics studies have been discussed in detail in the following sub-sections.

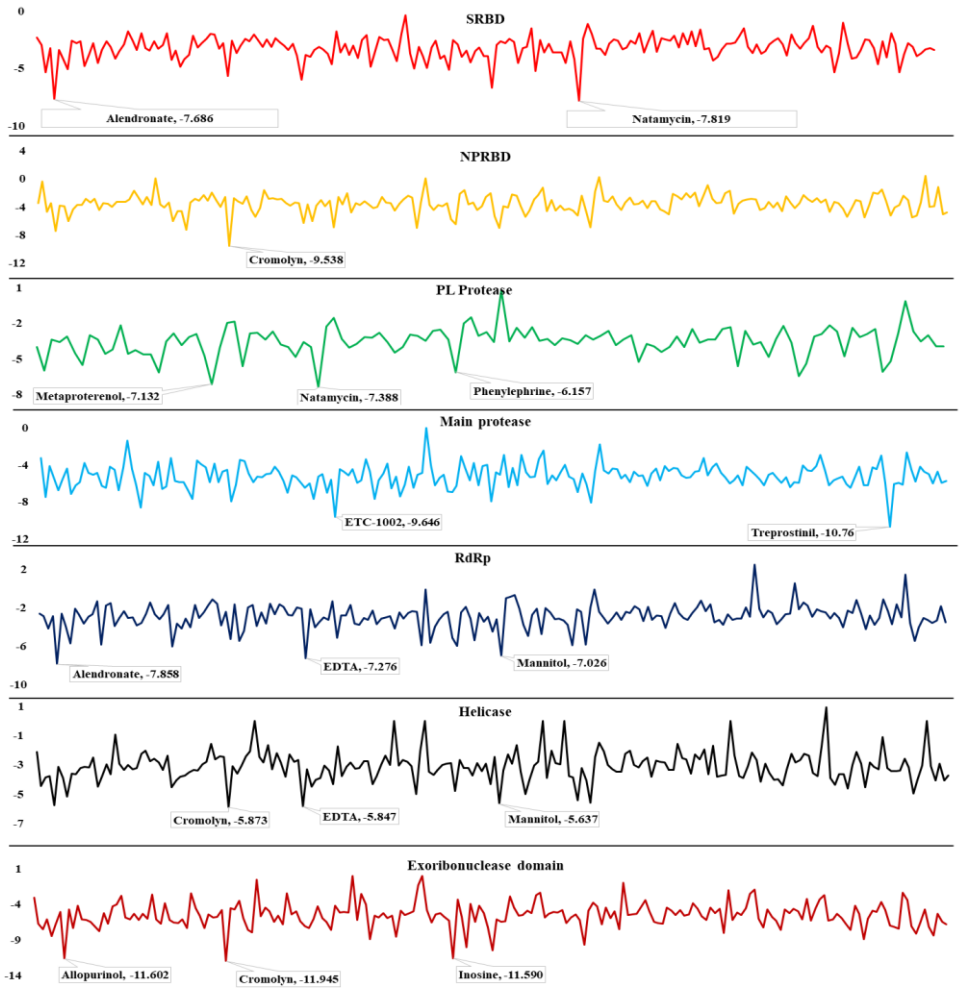

Figure 3: Docking score plot of all drugs against seven different targets; y-axis is docking score (in kcal/mol)

Table 3: Docking results of top four drugs against seven chosen targets

S. No	Target code	Drug name	Dock score (kcal/mol)	Type of interactions	Interacting residues – Bond length (in Å)
1.	Spike receptor binding domain (6M0J)	Natamycin	-7.82	H-bond	Tyr449: 1.97; Tyr453: 1.98; Gln498: 1.92; Asn501: 1.99, 2.46; Gly502: 2.15
		Alendronate	-7.69	H-bond	Arg403: 1.95; Tyr453: 2.10; Ser494: 1.78, 1.9, 1.8; Gly496: 1.95
2.	Nucleocapsid protein RNA binding domain (6VYO)	Cromolyn	-9.54	H-bond	Ala154(A): 1.99; Asn55(D): 2.09; Ala55(D): 2.17; Arg92(D): 2.45; Ala173(D): 1.79; Arg149(D): 1.98
				Salt bridge	Arg107(D): 4.33; Arg149(D): 3.87
3.	Papain Like protease (6W9C)	Natamycin	-7.39	H-bond	Asp(A) 108: 2.52; Lys157(C): 2.08; Leu162(C): 2.10; Gly163(C): 2.57; Glu167(C): 2.06
4.	Main protease (6W63)	Treprostinil	-10.76	H-bond	Cys44: 1.63; Glu166: 1.97; Thr190: 1.87; Gln192: 1.97
		Co-crystal	-6.90	H-bond	Gly143: 2.31; Asn142: 2.23; Hie163: 2.09; Glu166: 1.92
				π-π stacking	Hie41: 5.14
5.	RNA dependent RNA polymerase	Alendronate	-7.86	H-bond	Asp452: 1.95; Arg553: 1.94; Arg555: 2.64; Thr556: 1.61, 1.7, 1.83; Asp623: 1.76, 1.76
		Remdesivir	-3.27	H-bond	Asp618: 1.81, 1.98; Cys622: 2.66

	(6M71)			π-π stacking	Tyr455: 5.34
6.	Helicase (7NNG)	Cromolyn	-5.87	H-bond	Arg443: 2.14; Lys320: 2.23, 2.54; Gly538: 2.08
				π-cation	Arg443: 4.89, 4.81
		Co-crystal	-4.06	H-bond	Lys320: 2.15
				Salt bridge	Lys320: 2.88; Lys323: 2.96
7.	Exoribonuclease domain (7R2V)	Cromolyn	-11.95	H-bond	Leu366: 2.13; Tyr368: 1.99; Asn388: 1.85
				π-π stacking	Phe426: 4.2
		Co-crystal	-11.747	H-bond	Arg310: 1.83; Gly333: 1.99; Asp352: 1.78, 1.99; Ala353: 2.37; Tyr368: 2.01, 2.01; Trp385: 2.10
				Salt bridge	Arg310: 2.81

Table 4: Results of binding free energy studies of top four drugs

S. No	**Target code**	**Drug name**	**MM-GBSA (kcal/mol)**						
			dG Bind	**dG Bind coulomb**	**dG Bind covalent**	**dG Bind Hbond**	**dG Bind Lipo**	**dG Bind Solv GB**	**dG Bind vdW**
1	Spike receptor binding domain	Natamycin	-59.14	-49.54	9.53	-4.22	-13.83	27.86	-28.94
		Alendronate	-24.3	-38.01	5.9	-3.01	-3.05	20.98	-6.95
2	Nucleocapsid protein RNA binding domain	Cromolyn	-33.22	-305.11	8.83	-4.98	-2.57	305.5	-29.55
3	Papain Like protease	Natamycin	-37.19	-26.86	2.98	-2.41	-16.02	56.07	-50.95
4	Main protease	Co-crystal	-77.2	-29.4	6.49	-2.3	-19.52	34.76	-64.24
		Treprostinil	-65.67	-27.89	7.96	-2.93	-21.77	19.59	-39.38
5	RNA dependent RNA polymerase	Alendronate	-31.45	-65.06	8.96	-6.79	-1.74	43.8	-10.61
		Remdesivir	-26.03	-42.7	0.53	-3.17	-5.1	71.65	-44.69
6	Helicase	Co-crystal	-22.66	-25.61	0.51	-2.06	-5.65	37.85	-25.01
		Cromolyn	-48.39	-39.76	-1.16	-2.14	-2.92	50.68	-47.9
7	Exoribonuclease domain	Co-crystal	-56.93	-22.68	2.84	-6.29	-10.67	27.26	-46.87
		Cromolyn	-63.65	-27.14	8.88	-2.29	-9.77	27.78	-54.01

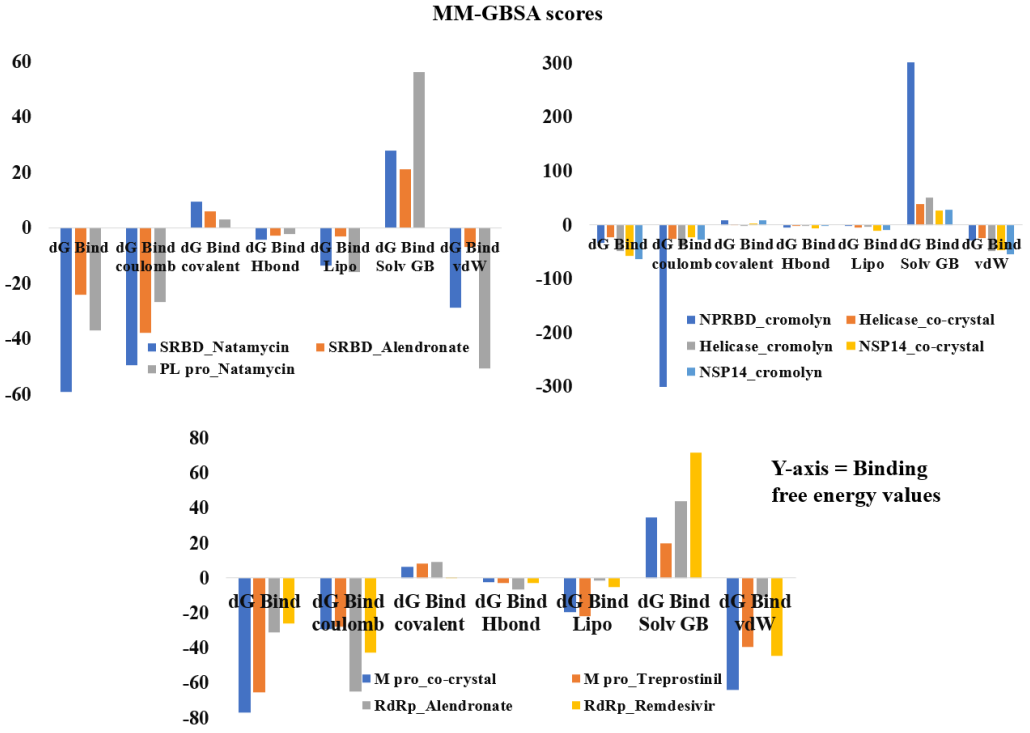

Figure 4: MM-GBSA scores of the top four drugs against the selected targets

Table 5. Pharmacological data of the top four drugs

S. No	Drug name	Original indication			
		Use	Mechanism of action	Target	IC_{50}/EC_{50}
1.	Natamycin	Antifungal	Fungal ergosterol inhibitor	Fungal cell membrane	25.66 µM (in MKN28 cells) [48]
		Antiviral	Not available	SARS-CoV-2	24.3 µM [49]
2.	Cromolyn	Anti-Asthmatic	Mast cell stabilizer	GPR35 (rat)	6.01 pEC50 [50]
3.	Alendronate	Anti-fracture	Farnesyl pyrophosphate synthase inhibitor	FNTB_HUMAN	7.30 (pIC50) [50]
4.	Treprostinil	Anti-thrombotic; Anti-inflammatory; Vasodilator	Prostanoid receptor (DP1 and EP2) agonist	P2RY12; PPARD; PTGIR	EC50 0.6 nM (DP1) 6.2 nM (DP2) [51]

3.3. Spike receptor binding domain (RBD)

Spike protein is a homotrimer with two subunits, namely S1 and S2 in each of the monomer. S1 contains the RBD which binds specifically to the host ACE2 to enable entry into the cells, and is prone to key mutations found in the different variants of concern [52]. On the other hand, S2 subunit arbitrates the viral-cell fusion followed by viral replication by infusing the viral genetic material [53,54]. Therefore, blocking the S1 subunit will help prevent the fusion with ACE2, preventing the viral entry and its replication. When we carried out the docking studies of the shortlisted drugs with the viral spike protein (PDB: 6M0J) by giving key interacting residues with ACE2 as the active site grid, the drugs natamycin and alendronate had the least docking score of -7.82 kcal/mol and -7.69 kcal/mol respectively, making them promising candidates. Additionally, the MM-GBSA scores of natamycin was -59.14 kcal/mol whereas for alendronate, it was -24.13kcal/mol. The residues Tyr449, Tyr453, Ser494, Gln498, Asn501 and Gly502 have shown interactions with natamycin. Among these, most of the interactions are due to hydroxyl groups of the drug. Only two residues

Ser494 and Tyr453 interacted with the 4-amino group of mycosamine sugar moiety. Interestingly, these residues are among those that interacted with the ACE2 receptor during viral entry [55]. As, natamycin binds to the same residue competitively, it prevents the binding of the ACE2 receptor. Similar binding pattern is seen in the case of alendronate, wherein the residues Arg403, Tyr453, Ser494 and Gly496 interacts with this drug. Therefore, due to better binding scores, there is a chance that these two drugs could prevent the entry of virus as well as inhibit the spike protein from viral replication.

To determine the behavior of ligand in a biological system, we used molecular dynamics simulation and found that natamycin was stable for the initial 20ns as the residue from the docked complex was retained during this period, but the ligand started losing few contacts after 20ns and moved slightly out of the active site pocket resulting in the increased RMSD and deviations until 60ns. After that, the ligand had consistent interactions with Asn437, and to a lesser extent with Asn440, until the end of the simulation time. As shown in Figure 5, the active site residue has low deviations in the random mean square fluctuations (RMSF) plot; c.f. time frame analysis for pose view at different time frames of natamycin (**supplementary Figure S2.1**). A different trend was observed in case of alendronate, wherein, the complex was stable for the initial 3ns and the contacts were same as that of docked complex. After 3ns, the molecule completely moved out of the assigned active site resulting in escalated RMSD to 60 Å and then declined to 32 Å at 5ns. During this, alendronate deviated from the active site and attached to the other side of the S1 protein by interacting with Asp427 and Asp428 (**c.f. time frame analysis, supplementary Figure S2.1**). Multiple strong interactions were seen with Asp427 and 428 while few contacts were observed with Phe429 and Thr430. From 6ns, the ligand was stable and the interactions with Asp427 and Asp428 were retained until the end of the simulation with minor deviations. As natamycin stays in the pocket till the end of simulation, it is most likely to inhibit the spike protein, and *in vitro* studies could show promising results.

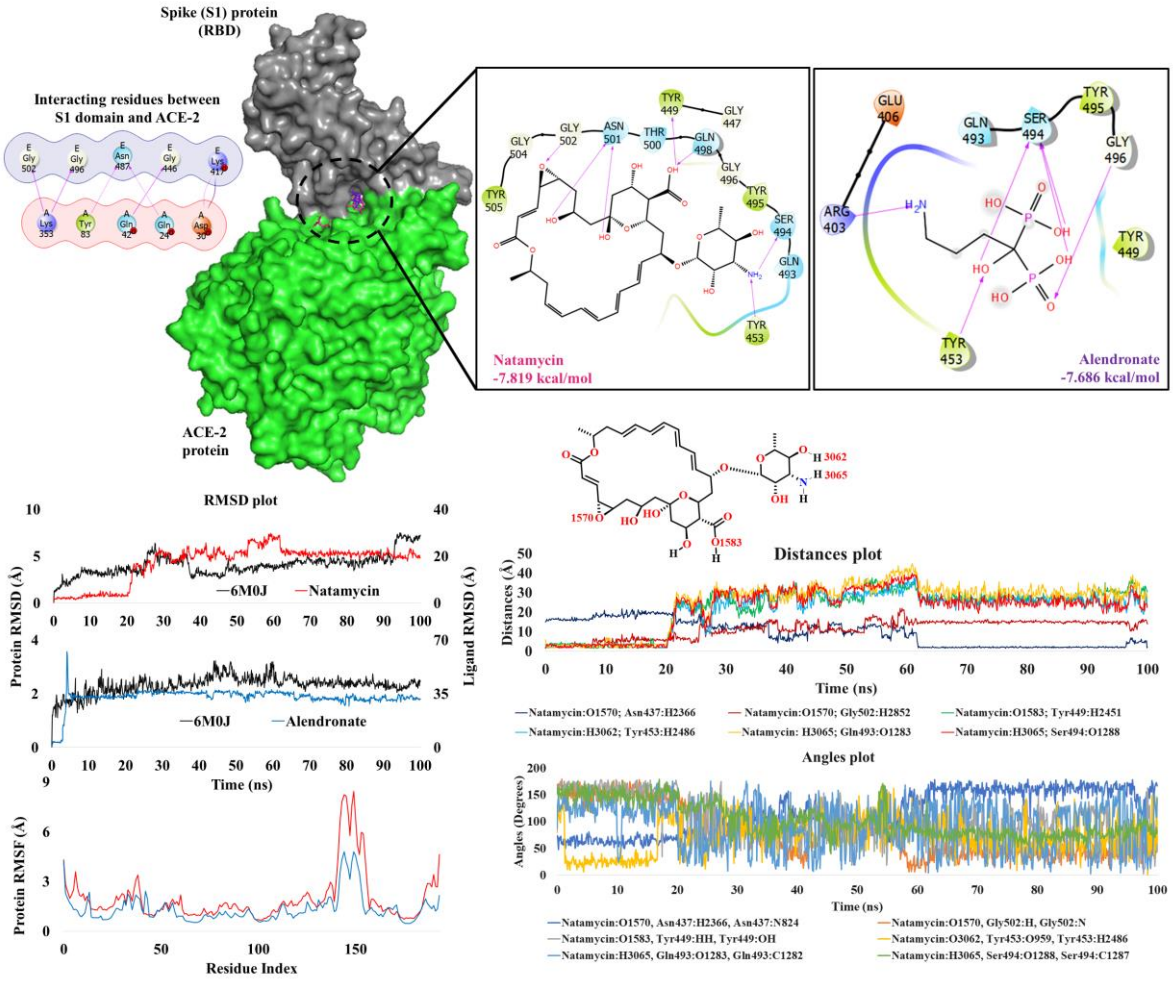

Figure 5. Docking result of natamycin and alendronate (top), RMSD and RMSF plots showing fluctuations in natamycin, alendronate and spike protein residues (left bottom), distances and angle plot between the atoms of interacting residues with natamycin during the entire simulations (right bottom)

3.4. *Nucleocapsid protein RNA binding domain (NPRBD)*

Nucleocapsid protein has a significant role in the viral structure as it binds to the virus's genetic material (RNA) and facilitates the folding process of hammerhead ribozyme that catalyzes reversible cleavage and ligation reaction at specific RNA sites. This results in preventing the formation of unproductive conformations of the RNA and production of a helical ribonucleoprotein. Further, it also regulates various cellular processes such as, cell cycle progression, apoptosis and actin reorganization [56]. The nucleocapsid protein has two different domains which aid in different functions. The N-terminal domain (NTD) is very important in case of viral replication and transcription; while the C-terminal domain (CTD) has conserved dimerization mechanisms by forming hydrophilic and hydrophobic interactions [56]. Since, N-protein has a major role in viral replication, inhibition of this target can be beneficial for treating SARS-CoV-2 infection. Upon performing docking with NPRBD (PDB: 6VYO), the drug with the best score was found to be cromolyn, a mast cell stabilizer with the docking score of -9.54 kcal/mol and MM-GBSA score of -33.22 kcal/mol. The residues that interacted with cromolyn include Ala55, Asn77, Arg92, Arg107, Arg149, Asn154 and Ala173. Except for Ala55, Asn77 and Ala173, all other residues interacted with the carboxyl terminals of the drug's chromene moiety, while the other residues (Asn77 and Ala173) interacted with the hydroxyl at 2nd position of propane linker, and Ala55 interacted with the moiety's keto group at the 4th position.

MD analysis of cromolyn in complex with 6VYO shows good RMSD plot as consistent deviations were observed with the protein residues. For the initial 48ns, the ligand has slight variations between RMSD of 3 Å-5 Å, during which the residues Trp52, Asn153, Asn154, Ala155 of chain A and Ala55, Thr57, Arg107, Tyr109, Arg149, Pro151, Ala156 and Asa173 of chain D showed strong interactions with the cromolyn molecule. After that, some of the interacting residues with the ligand were broken, resulting in escalated RMSD between 6 Å-10 Å up to 75ns (Figure 6).

Time frame analysis between 48ns-100ns shown (**supplementary Figure S2.2**) reveals that the ligand started uprooting from the binding site and was prevented to move away by the strong interactions of Arg107 and Arg149 which held the cromolyn molecule within the site. The alkyl chain (hydroxyl at the 2nd position of propane) linker between two chromene moieties were likely responsible for these higher deviations. The protein had a similar pattern as that of the ligand. Thr76 of chain A formed a new interaction while the residues Asn154, Ala155 of chain A and Arg107, Arg149 of chain D retained their strong interactions with the cromolyn molecule until the end of the simulation. Further, from the timeline plot, it is clear that the residues Arg107, and Arg149 of chain D contributed to most of the interactions while the other residues only made moderate contributions along with water mediated interactions **(c.f. 3.2-cromolyn, supplementary file S3).**

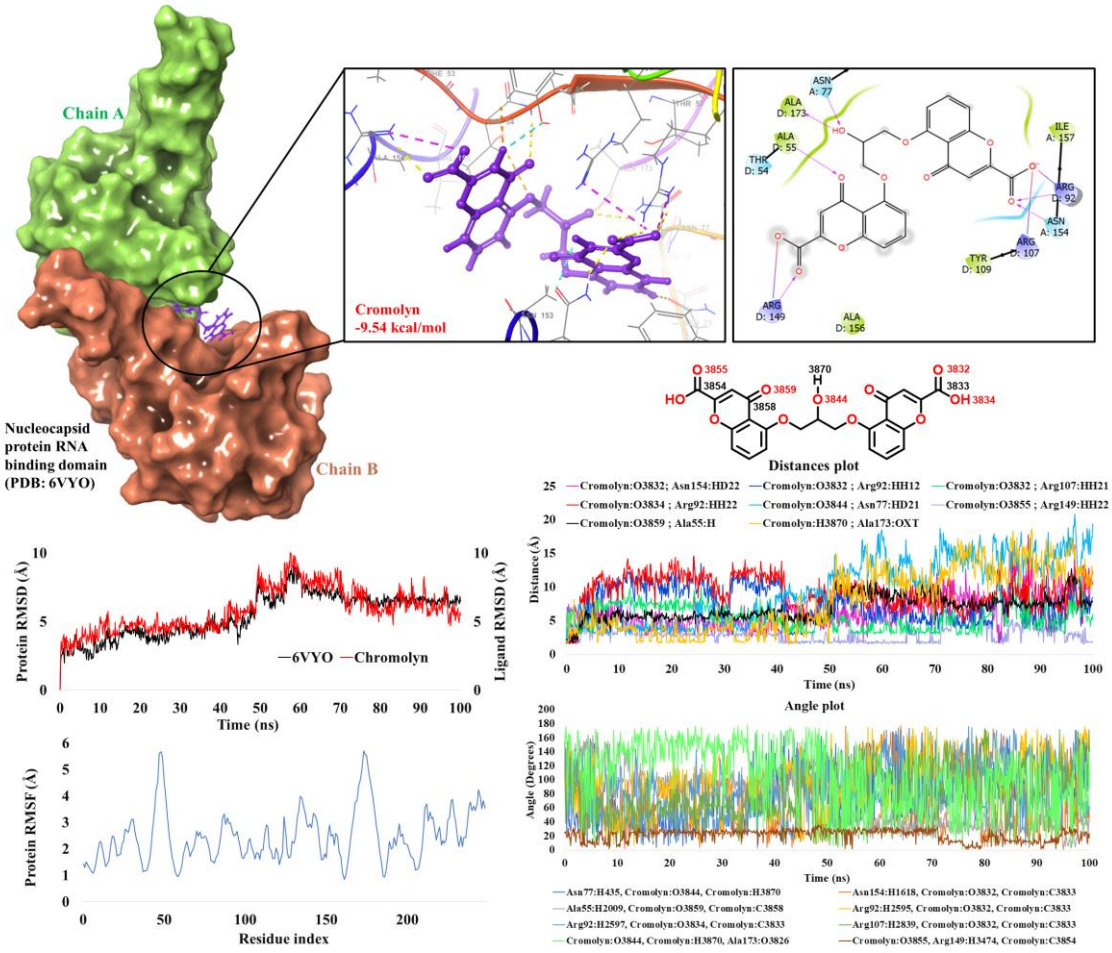

Figure 6. Docking result of cromolyn (top), RMSD and RMSF plots showing fluctuations in cromolyn and nucleocapsid protein (left bottom), distances and angle plot between the atoms of the interacting residues with cromolyn during the entire simulations (right bottom)

3.5. Papain like protease (PL pro)

PL proteases are multifunctional enzymes essential for the replication of viruses. It is capable of recognizing and hydrolyzing ubiquitin and Interferon-stimulated gene 15 (ISG15; Ubiquitin-like protein) that covalently form an isopeptide bond with the target protein, thereby favoring the entry/replication of the viral cells within the host. Hence, inhibiting PL pro could be a good approach to prevent the viral replication in the host system [57]. From our studies, three drugs, natamycin, alendronate and metaproterenol, were found to have close docking scores of -7.39 kcal/mol, -7.16 kcal/mol and -7.13 kcal/mol respectively. The active site of PL pro is between two chains (A and C) that gives a proper shape for the ligand to fit. Between these two chains, the residues that interacted with natamycin include Asp108 of chain A and Lys157, Leu162, Gly163 and Glu167 of chain C. The hydroxyl on the 25th carboxylic group of natamycin interacted with Lys157 and Leu162, while hydroxyl groups at 1st and 26th positions interacted with Gly163 and Asp108 respectively. Additionally, the hydroxyl at 6th position of the substituted sugar (mycosamine) interacted with Glu167. The MM-GBSA score of natamycin was found to be -37.19 kcal/mol

Further MD analysis shows low fluctuations of the target residues and the ligand during the complete simulation as the RMSD was <3.2 Å. After major fluctuations during 18-24ns and 44-56ns, the protein residues attained equilibrium for the rest of the simulation time. Change in Natamycin's conformation from the docked pose resulted in the RMSD of 4 Å, and we observed at 1ns that the residue Gln269 formed a contact with the drug, while Asp108 and Asn109 formed water mediated interactions. The fluctuations were varying up to 7 Å until 30ns; during 31ns-34ns and 40ns-48ns, the ligand had no contact with the protein (resulting in a higher RMSD of 12 Å). After 48ns, Tyr268 and Asn109 formed contact with natamycin resulting in decline of RMSD to 9 Å, and the ligand attained equilibrium as the fluctuations were not high towards the end. RMSF analysis shows low fluctuations of the residues except those in the active site region due to drug interaction. The residues 266-270 formed interactions with the ligand and resulted in higher RMSF due to fluctuations of the interacting atoms of the ligand (>4.0 Å) (Figure 7). The residues that were in contact predominantly with natamycin were Trp106, Asp108, Asn109, Asn267 and Tyr268. Among these, Asp108 and Asn267 retained the interactions and prevented the ligand from moving outside the active site (**c.f. supplementary Figure S2.3**). These two residues contributed to bulk of the simulation time (42% and 31% respectively), compared to Asn109, Thr265 and Tyr268 (10-15%).

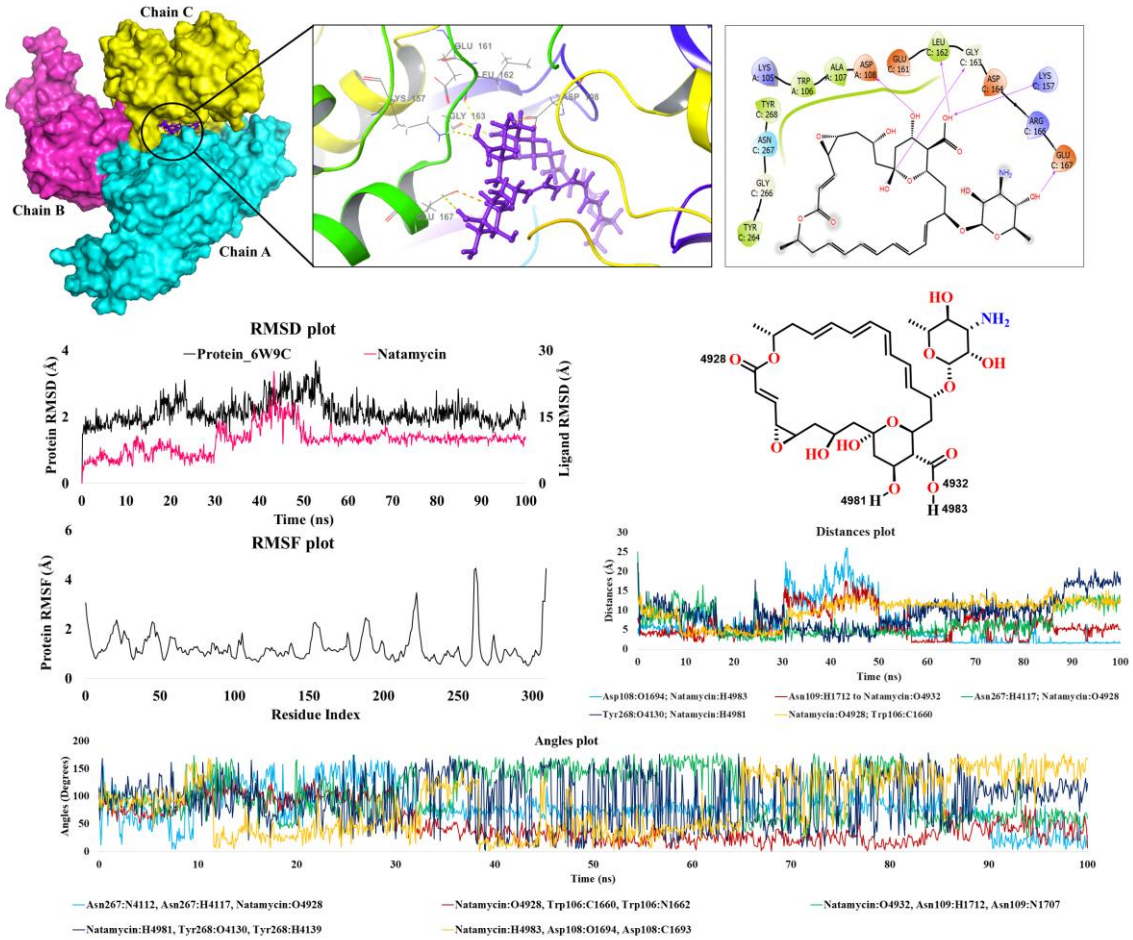

Figure 7. Docking result of natamycin (top), RMSD and RMSF plots showing fluctuations of natamycin and papain like protease (left bottom), distances and angle plot between the atoms of the interacting residues with natamycin during the entire simulations (right bottom)

3.6. 3CL Protease / Main protease

3CL protease, a C30 endopeptidase is found in almost all coronavirus variants and is involved in cleaving polyprotein at different conserved sites [58]. It possesses three major domains (D1, D2 and D3) and the active site remains between D1 and D2 [59]. From our docking analysis, a total of 14 drugs were found to have docking score close to the co-crystal ligand (-6.89 kcal/mol and MM-GBSA score -77.20kcal/mol). Among these, two drugs were found to have docking score > -9.0 kcal/mol. These two drugs are treprostinil, a prostacyclin vasodilator, and ETC-1002 (bempedoic acid), an anti-hyperlipidemic agent, with docking scores of -10.76 kcal/mol and -9.65 kcal/mol, and their MM-GBSA scores were -65.67 kcal/mol and -42.73 kcal/mol respectively. Since, treprostinil had the better score, we analyzed its binding pattern further. Treprostinil formed a total of four H-bonds each with Cys44 and Glu166, and two interactions each with Thr190 and Gln192. The hydroxyl group at 3rd position on the octyl side chain interacted with the carbonyl group of Thr190 and amino group of Gly192. In addition, the hydroxyl group at 2nd position of the cyclopentanaphthalene interacted with Glu166 and the carboxylic terminal of treprostinil formed H-bond with Cys44.

To understand the behavior of treprostinil, the docked pose of co-crystal ligand as well as treprostinil along with the protein was taken forward for molecular dynamics. During the simulation process, the fluctuations were low as the RMSD was below 3 Å. The RMSD of the protein corresponding to treprostinil is relatively less compared to the co-crystal,

indicating greater stability of the complex. Further, the ligand RMSD plot shows that co-crystal ligand had less RMSD than treprostinil until 50ns, however, huge deviations were observed until the end of the simulation. Treprostinil had RMSD ranging between 2 Å-4 Å until 35ns, beyond which the RMSD increased to 4 Å from 37ns and attained equilibrium until the end of the study. The residues that predominantly interacted with the ligand during the simulation process include Asp187, Gln189, Thr190 and Gln192. Additionally, these active site residues have fewer fluctuations during the simulation time as their RMSF is below 2 Å (Figure 8). Among these residues, Asp187, Thr190 contributed for >40% of interaction while Glu166, Arg188, Gln189 and Gln192 contributed for interactions ranging between 10% and 20%. The confirmations between 34ns-37ns were also captured as the ligand had slightly increased the RMSD during this interval, and it was observed that the drug was retained within the active site (**supplementary Figure S2.4**). As treprostinil has far better docking score than the co-crystal ligand, and the complex is more stable, it can be considered a potential candidate to target main protease experimentally.

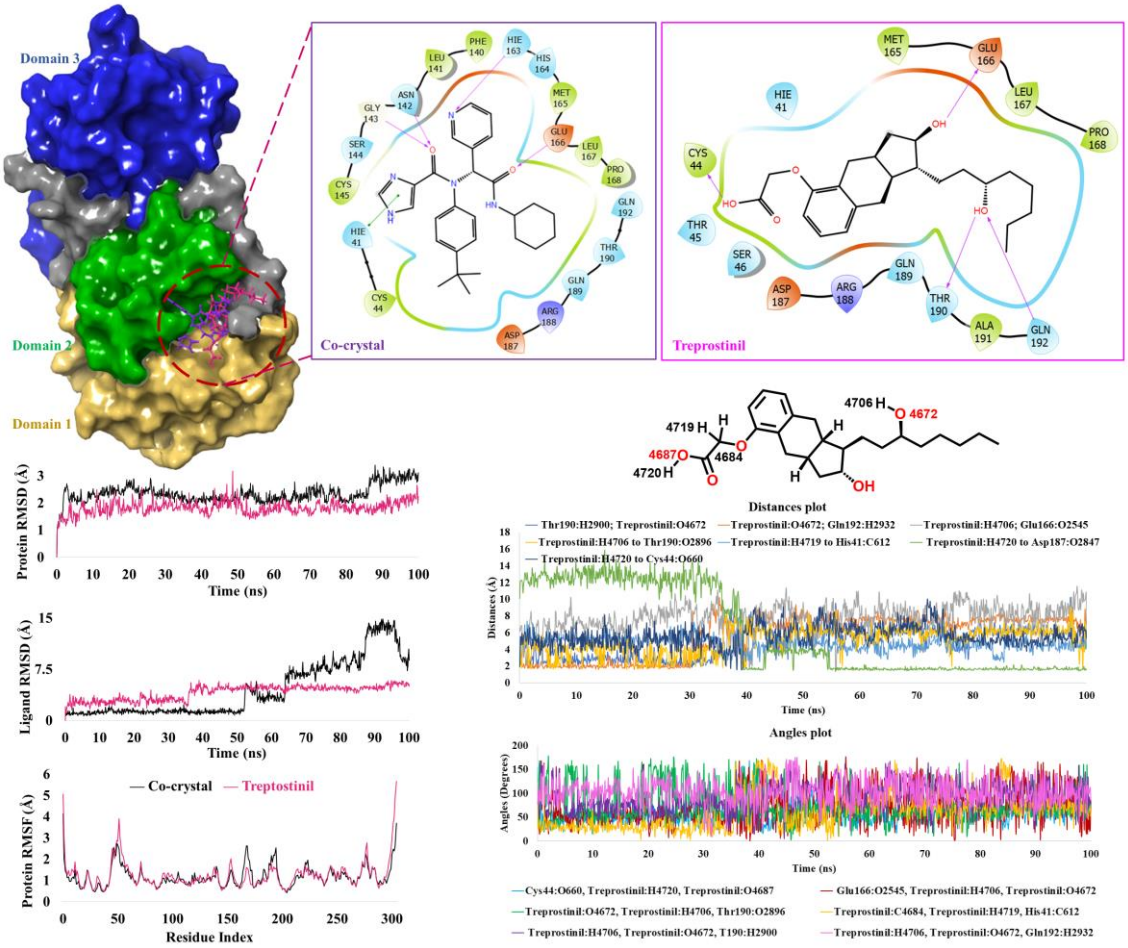

Figure 8. Docking result of co-crystal (top), RMSD plots of co-crystal and treprostinil, and RMSF plots showing fluctuations in 3CL protease (left bottom), distances and angle plot between the atoms of the interacting residues with Treprostinil during the entire simulations (right bottom)

3.7. RNA dependent RNA polymerase (RdRp)

RNA dependent RNA polymerases are highly conserved proteins and catalyze the replication process of an RNA template. The amino acids Asp760 and Asp761 are necessary for RNA synthesis, which binds to the 3′ end of RNA. Therefore, inhibiting this target could help in preventing the replication of the viral genetic material, thereby reducing the viral load [60]. When we performed the docking studies with the shortlisted ligands, alendronate, a

bisphosphonate drug, had the significant binding score of -7.86 kcal/mol (MM-GBSA: -31.45 kcal/mol), better than the control drug remdesivir's score of -3.27 kcal/mol (MM-GBSA: -26.03 kcal/mol). Alendronate was able to form a total of eight interactions each with Asp452, Arg553, Arg555, two with Asp623, and three with Thr556. All the interactions are due to the functional groups present on the bisphosphonate molecule. On the other hand, remdesivir had only one H-bond interaction with each of Asp618, Pro620 and Cys622. Tyr455 also formed π-π stacking interaction with the drug due to aromaticity.

MD studies of the alendronate complex with RdRp reveals a stable RMSD plot. Although it varied from its docking pose at 1ns, the interacting residue was still in contact with alendronate resulting in escalated RMSD to 6 Å and greater stability with low 4 Å – 6 Å fluctuations until 80ns. Asp623 and Asp760 had constant interactions with alendronate while Arg553, Arg555, Asp618, Lys621 and Cys622 had partial interactions. Beyond 80ns, the ligand further changed its conformation resulting in higher RMSD. The ligand for the last 20ns showed partial interactions with Arg553, Lys621, and Cyc622 while multiple strong interactions were seen with Asp618 and Asp623. The interactions with Asp760, an important residue for RNA synthesis, has strong interactions for the entire simulation but slightly decreased at the end of the study. RMSF plot shows minor fluctuation in the active site residues (<2.5 Å), indicating protein stability. The LP contact plot shows Asp623 and Asp760 contributed 87% and 77% respectively, to the total interactions. Contributions of other residues such as Arg553 (36%), Arg555 (22%), Asp618 (21%), Lys621 (34%) and Cys622 (24%) were moderate. The time frame analysis also shows the interaction of Asp623 and Asp760 during the fluctuating intervals (**supplementary Figure S2.5**).

To compare our results with the control drug, MD analysis was carried out. In our analysis, remdesivir was stable for the initial 10ns with RMSD 4 Å - 4.5 Å, followed by fluctuations, especially at 20ns - 45ns up to 9 Å, then a drop in RMSD of 6 Å-7 Å during 45ns-55ns, and equilibrium for the rest of the simulation. The protein was also stable as the interacting residues were within the RMSF of 2.0 Å (Figure 9). The timeline plot shows minor contributions of the residues during the simulation study, unlike alendronate complex (**c.f. 3.5-remdesivir, supplementary file S3**). While the key interacting residues of RdRp were present in the MD study of remdesivir, the interactions with alendronate were much stronger. The residue that participated in the direct interactions with remdesivir include Ala550 (20%), Arg555 (11%), Asp623 (13%) and Asp760 (20%) with moderate to low contributions. Alendronate had multiple stronger interactions with the active site and the drug remained within the active site during the entire simulation.

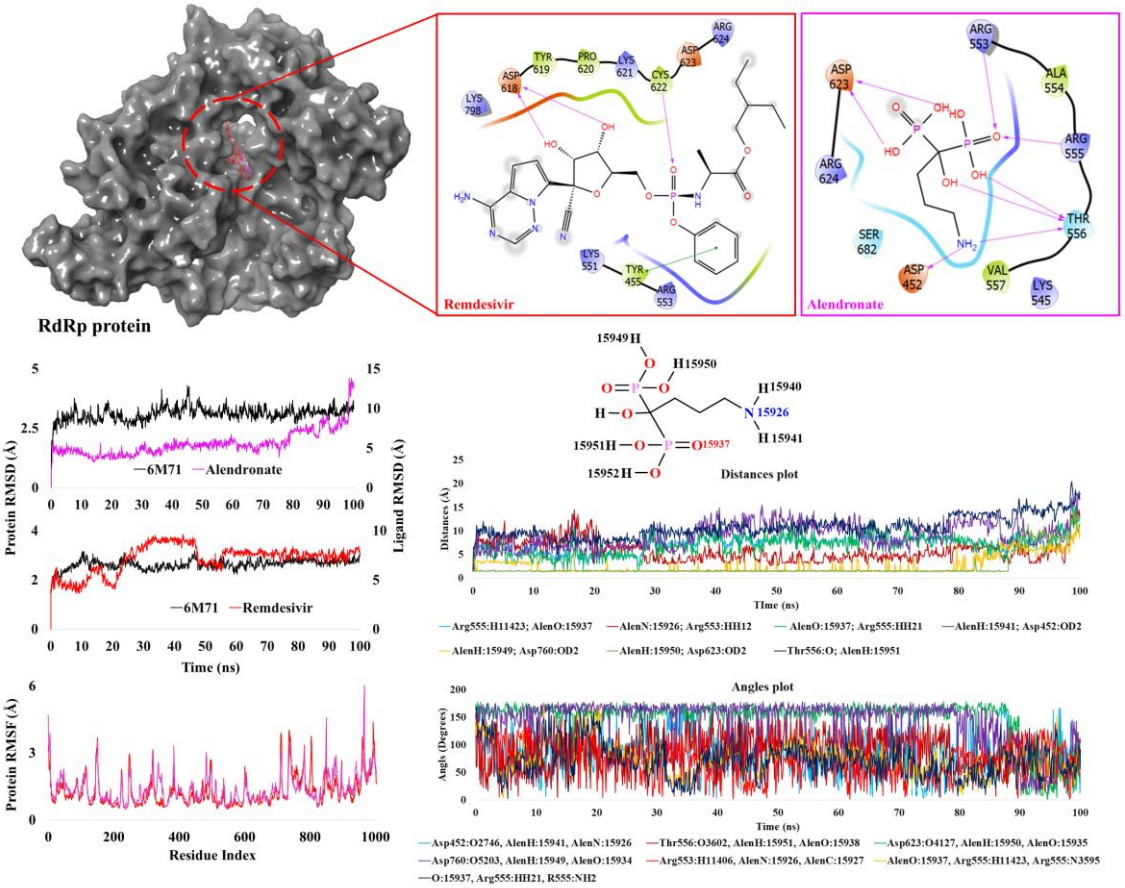

Figure 9. Docking result of Alendronate and remdesivir (top), RMSD plot of alendronate and remdesivir, and RMSF plots showing fluctuations RdRp protein (left bottom), distances and angle plot between the atoms of the interacting residues and Alendronate during the entire simulations (right bottom)

3.8. Helicase

Helicases are the enzymes responsible for unwinding of helical structure of genetic material producing ssDNA / ssRNA that is essential for 3R's (replication, recombination and repair) [9,10]. The unwinding process occurs by breaking the H-bonds sequentially between two strands of the double helix and this whole process of bond breaking is catalyzed by ATPase that consumes a molecule of ATP and produces sufficient energy to break the bond [61]. Hence, preventing the bond breaking could halt the unwinding process and thus the 3R's. As these enzymes are highly conserved across all coronaviruses, it is an interesting target to block the viral replication [62]. Upon docking of the shortlisted 214 FDA/TGA approved drugs, the molecule with best binding score was found to be cromolyn (-5.87 kcal/mol) with MM-GBSA core of -48.39 kcal/mol which is slightly better than the co-crystal ligand (-4.02 kcal/mol) with MM-GBSA score of -22.66 kcal/mol. The residue that participated in interactions with cromolyn were Lys320, Arg443 and Gly532, while only Lys320 was involved in interacting with the co-crystal ligand.

RMSD plot from our MD studies reveal initial fluctuations followed by stability. Although Glu261, Ser289, Thr440, Arg442, and Glu540 were not in interaction in the docked complex, they were found to interact with the ligand during the first 5ns of MD studies leading to RMSD of 6 Å. Between 10ns-35ns the ligand fluctuated to 10 Å after which it attained equilibrium. During this, the protein active site residues had minor fluctuations (<2 Å) as shown in the RMSF plot. Beyond 35ns, Glu261 contributed significantly (64%) and other residues moderately (15%-20% for Asp260, Asn268, Phe291, Phe437, Thr440, Lys462 and His464) to ligand bonding. Two π-cation interactions were also seen with His290 (10%) and His464 (11%). Despite fluctuations, the ligand never left the active site during the entire simulation (**c.f. time frame analysis, supplementary Figure S2.6**). When we performed the MD studies to the co-crystal ligand, the RMSD trend was similar to that of cromolyn as RMSD escalated between 7 Å-8 Å for the first half of the simulation time and then declined to 6 Å (Figure 10). All the interacting residues with the co-crystal ligand were within the active site region and the major contributing residues include His290 (33%), Lys320 (76%), Tyr324 (30%), Arg443 (94%) and Lys569 (15%). Since cromolyn and the co-crystal ligand have similar behavior during the simulation, both molecules could have similar potency.

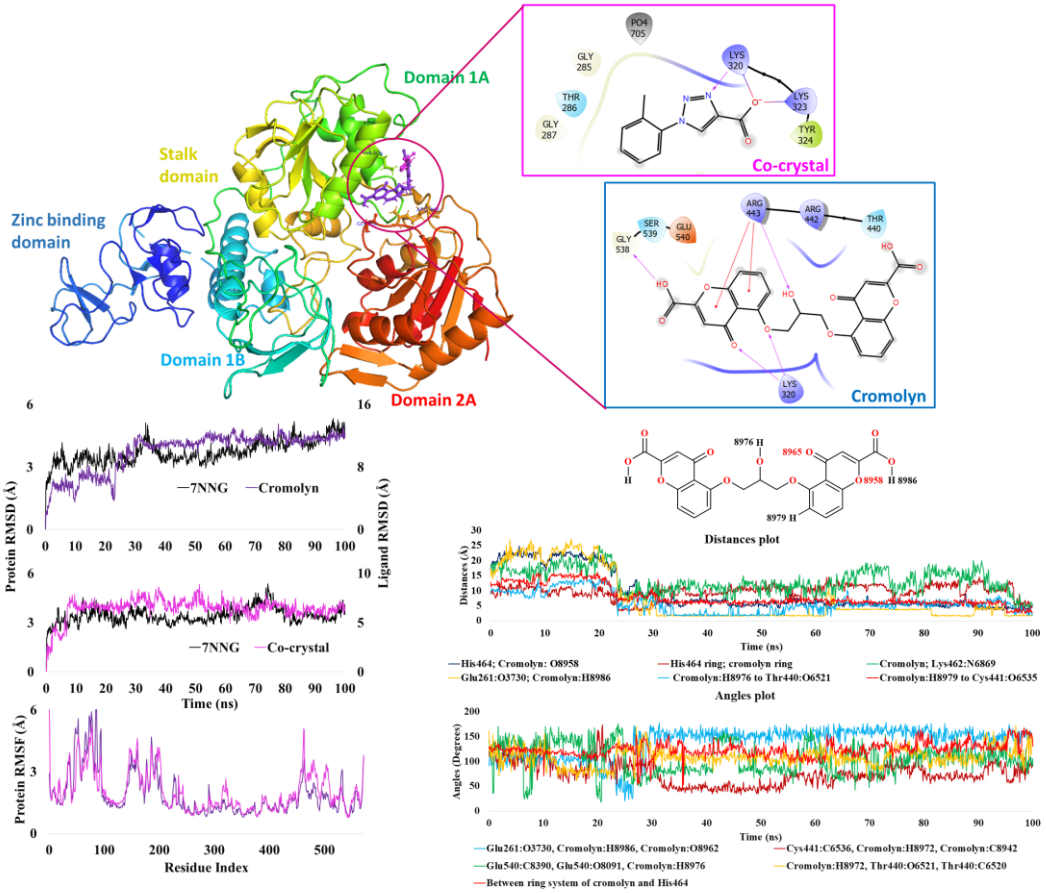

Figure 10. Docking result of co-crystal and cromolyn (top), RMSD plot of co-crystal and cromolyn, and RMSF plots showing fluctuations helicase protein (left bottom), distances and angle plot between the atoms of the interacting residues with the cromolyn during the entire simulations (right bottom)

3.9. Exoribonuclease domain

NSP14 has two terminals with different activities; the N-terminal has 3'-5' exoribonuclease activity, while the C-terminal has N7-methyl transferase (MTase) activity [63]. While the C-terminal preserves the stability of the viral RNA, the N-terminal role is crucial for maintaining the RNA genome [64]. To exhibit MTase activity, NSP14 uses S-Adenosyl methionine (SAM) as a methyl donor that causes methylation on the Nitrogen at the 7th position of guanine (5' end), which is necessary for mRNA stability as well as the translation process in human cells [65]. Therefore, by introducing a molecule with more affinity to the active site residues than the SAM, it is possible to block the activity of

MTase. When we performed docking studies with this protein (PDB: 7R2V), three drugs had scores closer to the co-crystal (docking score: -11.75 kcal/mol and MM-GBSA score: -56.93 kcal/mol). These drugs were cromolyn (docking score: -11.95 kcal/mol; MM-GBSA score: -63.65 kcal/mol), allopurinol (docking score: -11.60 kcal/mol; MM-GBSA score: -47.66 kcal/mol) and inosine (docking score: -11.59 kcal/mol; MM-GBSA score: -50.44 kcal/mol). Since cromolyn had a better score, we further analyzed it in terms of interactions. The S-Adenosyl homocysteine (SAH) ligand showed interactions with Arg310, Asp352, Ala353, Tyr368 and Trp385. Unlike the SAH, cromolyn had different interacting residues such Tyr368, Asn386 and Asn388. However, the binding site residues were the same in all three drugs. As cromolyn had the best score, MD studies were conducted to analyze its behavior and compare its binding properties with that of the co-crystal ligand.

MD analysis of cromolyn shows RMSD ranging between 1.5 Å - 6.4 Å, and interactions with Asn306, Leu366, Tyr368, Asn388 and Phe426 until 12ns. After 16ns, water-mediated interactions were mainly observed and the RMSD was between 3 Å-6 Å. RMSF plot shows that active site residues in cromolyn complex had similar pattern to that of the co-crystal. During the simulation, key contributing residues were Asn306 (62%), Trp385 (34%), Tyr420 (58%) and Phe426 (24%). Time frame conformations of the ligand were captured to see the binding pose at different fluctuating intervals **(supplementary figure S2.7).** It is observed that the change in the conformation was due to cromolyn's rotatable bonds. When we compared the results with co-crystal ligand, the RMSD reveals fluctuations for the initial 5ns (RMSD 2.4 Å - 5.6 Å) which started to decline and attain equilibrium (fluctuations between 2.5 Å - 3 Å) towards the end of the simulation (Figure 11). The residue that contributed in the study include Gln313, Asp331, Ile332, Asp352, Tyr368, Trp385, Asn386 and Asn388. Among these, Asp352 (92%), Tyr368 (98%), Trp385 (74%) and Asn388 (41%) are especially important.

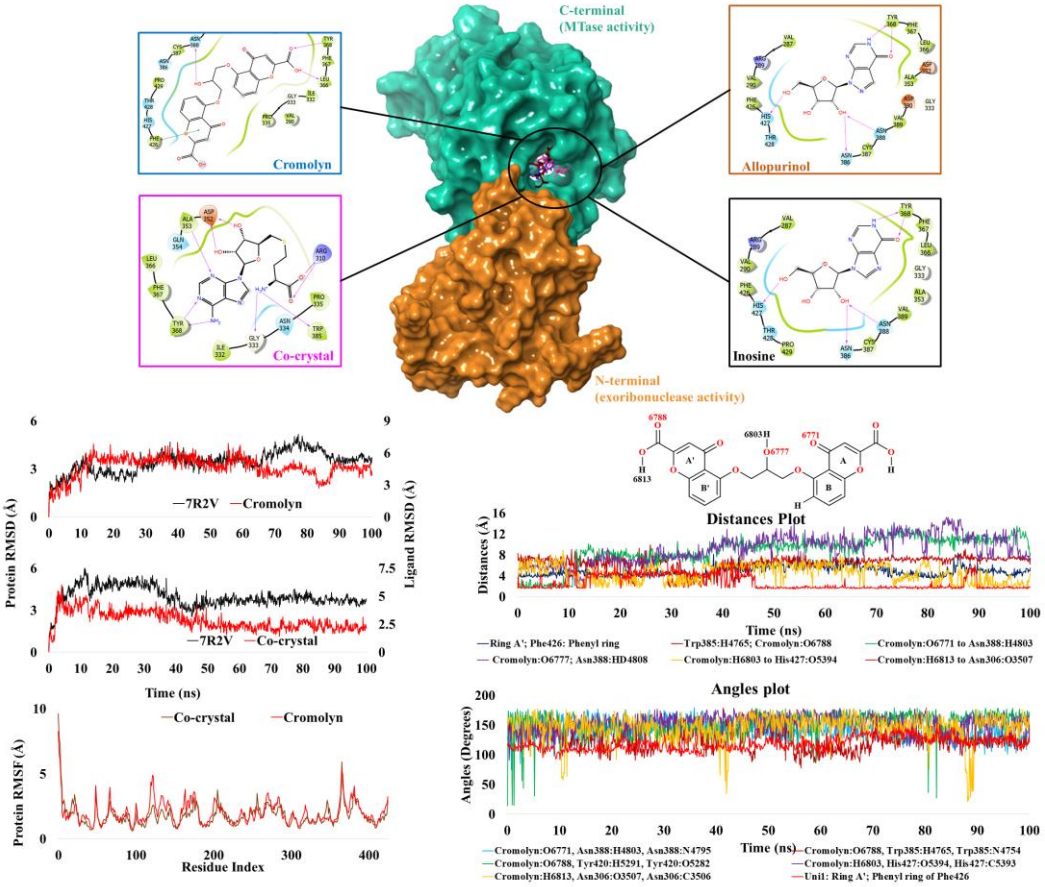

Figure 11. Docking result of co-crystal and cromolyn (top), RMSD plot of co-crystal and cromolyn, and RMSF plots showing fluctuations helicase protein (left bottom), distances and angle plot between the atoms of the interacting residues with the cromolyn during the entire simulations (right bottom)

4. Conclusions and future perspectives

From the molecular docking and molecular dynamics studies, it is clear that the drugs, treprostinil, natamycin, cromolyn and alendronate have shown promising results against various targets of SARS-CoV-2. RMSD plots and time frame analysis have revealed interesting behavior of these drugs during the simulation. In the case of main protease, treprostinil had a better RMSD plot when compared to the co-crystal ligand, with limited fluctuations. On the other hand, the fluctuations of natamycin and the residues in papain

like protease were similar, with interactions maintained until the end of the simulation. Cromolyn also shows interesting results with three different targets (N protein RNA binding domain, NSP13 and NSP14). It maintained constant interactions during the entire molecular dynamic simulation. Alendronate was able to form strong interactions with two targets (spike receptor binding domain and RNA dependent RNA polymerase). Its interaction with RdRp was far better than remdesivir, which is a current standard of care. From this study, we propose that these four drugs (treprostinil, alendronate, natamycin and cromolyn) could have antiviral effects and could be potential candidates to treat SARS-CoV-2 infections. As treprostinil promotes vasodilation of pulmonary and systemic arterial vasculature, it might have beneficial effects for COVID-19 patients through improving oxygenation and nitric oxide levels in the blood vessels, inhibiting platelet aggregation, and its anti-inflammatory property [66–68]. Our study further shows that this antihypertensive drug has better binding pattern than the co-crystal ligand. Alendronate is an amino-bisphosphonate indicated for osteoporosis, and patients administered with this drug have reportedly low incidences of COVID-19 testing and hospitalization [69,70], which could be due to their immunomodulatory effects and active site interactions as discerned in our study. Natamycin is an anti-fungal drug used in eye infections and we could find two publications pertaining to COVID-19; an *in-silico* study has suggested its use in combination with baloxavir marboxil and RU85053 as a cocktail as they inhibit 3CLpro, PL pro and RdRp; and an in-vitro study proves its antiviral activity with an EC_{50} of 24.3 µM [49,71]. Our simulation study shows significant binding interactions with PL pro and better dynamic behavior, thus strengthening its evidence base for further investigation. Our study shows that cromolyn, a mast cell stabilizer used as an asthma drug, is promising due to better binding score with multiple interactions and similar dynamic behavior to that of the co-crystal; unsurprisingly, it is currently in phase III COVID-19 clinical trial [72,73]. The study has identified four potential drugs – treprostinil, natamycin, cromolyn, and alendronate – as promising candidates against various targets of SARS-CoV-2 through molecular docking and molecular dynamics simulation. While the results are encouraging, it is crucial to emphasize that experimental validation through *in vitro* and *in vivo* studies is essential before considering these drugs for clinical use. The study does not advocate for the administration of these drugs with this preliminary study level without proper experimental data and regulatory approval. Further research is needed to conclusively

establish their antiviral effects and safety profiles, taking into account their potential interactions, dosages, and possible side effects. After validating through comprehensive *in vitro* and *in vivo* studies for their antiviral activity and safety profiles, suitable insights can be obtained that can serve as a starting point for further modifications of the chemical structure to enhance their binding affinity, improved absorption, distribution, metabolism, and excretion (ADME) profiles, and minimize potential interactions ensuring selectivity and reduced off-target effects. Additionally, these drugs can be considered components of possible combination therapies for treating or managing COVID-19. We are currently implementing the approach presented in this paper to our broader list of 1029 repurposed drug candidates and improving our methodology with better alternatives to the Tanimoto coefficient [37,74,75]. We are also extending our approach to the key variants of SARS-CoV-2 [52].

Acknowledgments
Authors are grateful to their respective institutions for internal funding and infrastructure. The article reflects the authors' views and does not represent the views or policies of any affiliating or funding agency. We thank our colleagues for their comments and support.

Conflict of Interest

The authors declare no conflict of interest.

References

(1) Mathieu, E.; Ritchie, H.; Rodés-Guirao, L.; Cameron, A.; Giattino, C.; Hasell, J.; Macdonald, B.; Dattani, S.; Beltekian, D.; Ortiz-Ospina, E.; Roser, M. *Coronavirus Pandemic (COVID-19)*. https://ourworldindata.org/coronavirus (accessed 2023-05-06).

(2) Wang, H.; Paulson, K. R.; Pease, S. A.; Watson, S.; Comfort, H.; Zheng, P.; Aravkin, A. Y.; Bisignano, C.; Barber, R. M.; Alam, T.; Fuller, J. E.; May, E. A.; Jones, D. P.; Frisch, M. E.; Abbafati, C.; Adolph, C.; Allorant, A.; Amlag, J. O.; Bang-Jensen, B.; Bertolacci, G. J.; Bloom, S. S.; Carter, A.; Castro, E.; Chakrabarti, S.; Chattopadhyay, J.; Cogen, R. M.; Collins, J. K.; Cooperrider, K.; Dai, X.; Dangel, W. J.; Daoud, F.; Dapper, C.; Deen, A.; Duncan, B. B.; Erickson, M.; Ewald, S. B.; Fedosseeva, T.; Ferrari, A. J.; Frostad, J. J.; Fullman, N.; Gallagher, J.; Gamkrelidze, A.; Guo, G.; He, J.; Helak, M.; Henry, N. J.; Hulland, E. N.; Huntley, B. M.; Kereselidze, M.; Lazzar-Atwood, A.; LeGrand, K. E.; Lindstrom, A.; Linebarger, E.; Lotufo, P. A.; Lozano, R.; Magistro, B.; Malta, D. C.; Månsson, J.; Mantilla Herrera, A. M.; Marinho, F.; Mirkuzie, A. H.; Misganaw, A. T.; Monasta, L.; Naik, P.; Nomura, S.; O'Brien, E. G.; O'Halloran, J. K.; Olana, L. T.; Ostroff, S. M.; Penberthy, L.; Reiner Jr, R. C.; Reinke, G.; Ribeiro, A. L. P.; Santomauro, D. F.; Schmidt, M. I.; Shaw, D. H.; Sheena, B. S.; Sholokhov, A.; Skhvitaridze, N.; Sorensen, R. J. D.; Spurlock, E. E.; Syailendrawati, R.; Topor-Madry, R.;

Troeger, C. E.; Walcott, R.; Walker, A.; Wiysonge, C. S.; Worku, N. A.; Zigler, B.; Pigott, D. M.; Naghavi, M.; Mokdad, A. H.; Lim, S. S.; Hay, S. I.; Gakidou, E.; Murray, C. J. L. Estimating Excess Mortality Due to the COVID-19 Pandemic: A Systematic Analysis of COVID-19-Related Mortality, 2020–21. *Lancet* **2022**, *399* (10334), 1513–1536. https://doi.org/10.1016/S0140-6736(21)02796-3.

(3) World Health Organization. *Monkeypox, COVID-19 & other global health issues virtual press conference - 22 September 2022*. https://www.who.int/publications/m/item/monkeypox--covid-19---other-global-health-issues-virtual-press-conference---22-september-2022 (accessed 2023-06-05).

(4) World Health Organization. *Weekly epidemiological update on COVID-19 - 28 December 2021*. https://www.who.int/publications/m/item/weekly-epidemiological-update-on-covid-19---28-december-2021.

(5) Mallapaty, S. China COVID Wave Could Kill One Million People, Models Predict. *Nature* **2022**. https://doi.org/10.1038/d41586-022-04502-w.

(6) Kakavandi, S.; Zare, I.; VaezJalali, M.; Dadashi, M.; Azarian, M.; Akbari, A.; Ramezani Farani, M.; Zalpoor, H.; Hajikhani, B. Structural and Non-Structural Proteins in SARS-CoV-2: Potential Aspects to COVID-19 Treatment or Prevention of Progression of Related Diseases. *Cell Commun. Signal.* **2023**, *21* (1), 110. https://doi.org/10.1186/s12964-023-01104-5.

(7) Yadav, R.; Chaudhary, J. K.; Jain, N.; Chaudhary, P. K. Role of Structural and Non-Structural Proteins and Therapeutic. *Cells* **2021**, *10* (4), 821. https://doi.org/10.3390/cells10040821

(8) Mariano, G.; Farthing, R. J.; Lale-Farjat, S. L. M.; Bergeron, J. R. C. Structural Characterization of SARS-CoV-2: Where We Are, and Where We Need to Be. *Front. Mol. Biosci.* **2020**, *7*. https://doi.org/10.3389/fmolb.2020.605236.

(9) Wu, Y. Unwinding and Rewinding: Double Faces of Helicase? *J. Nucleic Acids* **2012**, *2012*, 1–14. https://doi.org/10.1155/2012/140601.

(10) Ambrus, A. M.; Frolov, M. V. The Diverse Roles of RNA Helicases in RNAi. *Cell Cycle* **2009**, *8* (21), 3500–3505. https://doi.org/10.4161/cc.8.21.9887.

(11) Tahir, M. Coronavirus Genomic Nsp14-ExoN, Structure, Role, Mechanism, and Potential Application as a Drug Target. *J. Med. Virol.* **2021**, *93* (7), 4258–4264. https://doi.org/10.1002/jmv.27009.

(12) Ogando, N. S.; Zevenhoven-Dobbe, J. C.; van der Meer, Y.; Bredenbeek, P. J.; Posthuma, C. C.; Snijder, E. J. The Enzymatic Activity of the Nsp14 Exoribonuclease Is Critical for Replication of MERS-CoV and SARS-CoV-2. *J. Virol.* **2020**, *94* (23). https://doi.org/10.1128/jvi.01246-20.

(13) Lee, A. R. Y. Bin; Wong, S. Y.; Chai, L. Y. A.; Lee, S. C.; Lee, M. X.; Muthiah, M. D.; Tay, S. H.; Teo, C. B.; Tan, B. K. J.; Chan, Y. H.; Sundar, R.; Soon, Y. Y. Efficacy of Covid-19 Vaccines in Immunocompromised Patients: Systematic Review and Meta-Analysis. *BMJ* **2022**, 376: e068632. https://doi.org/10.1136/bmj-2021-068632.

(14) Turtle, L.; Thorpe, M.; Drake, T. M.; Swets, M.; Palmieri, C.; Russell, C. D.; Ho, A.; Aston, S.; Wootton, D. G.; Richter, A.; de Silva, T. I.; Hardwick, H. E.; Leeming, G.; Law, A.; Openshaw, P. J. M.; Harrison, E. M.; Baillie, J. K.; Semple, M. G.; Docherty, A. B. Outcome of COVID-19 in Hospitalised Immunocompromised Patients: An Analysis of the WHO ISARIC CCP-UK Prospective Cohort Study. *PLOS Med.* **2023**, *20* (1), e1004086. https://doi.org/10.1371/journal.pmed.1004086.

(15) Baek, M. S.; Lee, M.-T.; Kim, W.-Y.; Choi, J. C.; Jung, S.-Y. COVID-19-Related Outcomes in Immunocompromised Patients: A Nationwide Study in Korea. *PLoS One* **2021**, *16* (10),

e0257641. https://doi.org/10.1371/journal.pone.0257641.

(16) Wallace, B. I.; Kenney, B.; Malani, P. N.; Clauw, D. J.; Nallamothu, B. K.; Waljee, A. K. Prevalence of Immunosuppressive Drug Use Among Commercially Insured US Adults, 2018-2019. *JAMA Netw. Open* **2021**, *4* (5), e214920. https://doi.org/10.1001/jamanetworkopen.2021.4920.

(17) Gianfrancesco, M.; Hyrich, K. L.; Al-Adely, S.; Carmona, L.; Danila, M. I.; Gossec, L.; Izadi, Z.; Jacobsohn, L.; Katz, P.; Lawson-Tovey, S.; Mateus, E. F.; Rush, S.; Schmajuk, G.; Simard, J.; Strangfeld, A.; Trupin, L.; Wysham, K. D.; Bhana, S.; Costello, W.; Grainger, R.; Hausmann, J. S.; Liew, J. W.; Sirotich, E.; Sufka, P.; Wallace, Z. S.; Yazdany, J.; Machado, P. M.; Robinson, P. C. Characteristics Associated with Hospitalisation for COVID-19 in People with Rheumatic Disease: Data from the COVID-19 Global Rheumatology Alliance Physician-Reported Registry. *Ann. Rheum. Dis.* **2020**, *79* (7), 859–866. https://doi.org/10.1136/annrheumdis-2020-217871.

(18) Tomazini, B. M.; Maia, I. S.; Cavalcanti, A. B.; Berwanger, O.; Rosa, R. G.; Veiga, V. C.; Avezum, A.; Lopes, R. D.; Bueno, F. R.; Silva, M. V. A. O.; Baldassare, F. P.; Costa, E. L. V.; Moura, R. A. B.; Honorato, M. O.; Costa, A. N.; Damiani, L. P.; Lisboa, T.; Kawano-Dourado, L.; Zampieri, F. G.; Olivato, G. B.; Righy, C.; Amendola, C. P.; Roepke, R. M. L.; Freitas, D. H. M.; Forte, D. N.; Freitas, F. G. R.; Fernandes, C. C. F.; Melro, L. M. G.; Junior, G. F. S.; Morais, D. C.; Zung, S.; Machado, F. R.; Azevedo, L. C. P. Effect of Dexamethasone on Days Alive and Ventilator-Free in Patients With Moderate or Severe Acute Respiratory Distress Syndrome and COVID-19. *JAMA* **2020**, *324* (13), 1307. https://doi.org/10.1001/jama.2020.17021.

(19) National Institutes of Health. *Remdesivir*. *COVID-19 treatment guidelines*. https://www.covid19treatmentguidelines.nih.gov/therapies/antiviral-therapy/remdesivir/ (accessed 2023-06-06).

(20) Kozlov, M. Merck's COVID Pill Loses Its Lustre: What That Means for the Pandemic. *Nature* **2021**. https://doi.org/10.1038/d41586-021-03667-0.

(21) Butler, C. C.; Hobbs, F. D. R.; Gbinigie, O. A.; Rahman, N. M.; Hayward, G.; Richards, D. B.; Dorward, J.; Lowe, D. M.; Standing, J. F.; Breuer, J.; Khoo, S.; Petrou, S.; Hood, K.; Nguyen-Van-Tam, J. S.; Patel, M. G.; Saville, B. R.; Marion, J.; Ogburn, E.; Allen, J.; Rutter, H.; Francis, N.; Thomas, N. P. B.; Evans, P.; Dobson, M.; Madden, T.-A.; Holmes, J.; Harris, V.; Png, M. E.; Lown, M.; van Hecke, O.; Detry, M. A.; Saunders, C. T.; Fitzgerald, M.; Berry, N. S.; Mwandigha, L.; Galal, U.; Mort, S.; Jani, B. D.; Hart, N. D.; Ahmed, H.; Butler, D.; McKenna, M.; Chalk, J.; Lavallee, L.; Hadley, E.; Cureton, L.; Benysek, M.; Andersson, M.; Coates, M.; Barrett, S.; Bateman, C.; Davies, J. C.; Raymundo-Wood, I.; Ustianowski, A.; Carson-Stevens, A.; Yu, L.-M.; Little, P.; Agyeman, A. A.; Ahmed, T.; Allcock, D.; Beltran-Martinez, A.; Benedict, O. E.; Bird, N.; Brennan, L.; Brown, J.; Burns, G.; Butler, M.; Cheng, Z.; Danson, R.; de Kare-Silver, N.; Dhasmana, D.; Dickson, J.; Engamba, S.; Fisher, S.; Fox, R.; Frost, E.; Gaunt, R.; Ghosh, S.; Gilkar, I.; Goodman, A.; Granier, S.; Howell, A.; Hussain, I.; Hutchinson, S.; Imlach, M.; Irving, G.; Jacobsen, N.; Kennard, J.; Khan, U.; Knox, K.; Krasucki, C.; Law, T.; Lee, R.; Lester, N.; Lewis, D.; Lunn, J.; Mackintosh, C. I.; Mathukia, M.; Moore, P.; Morton, S.; Murphy, D.; Nally, R.; Ndukauba, C.; Ogundapo, O.; Okeke, H.; Patel, A.; Patel, K.; Penfold, R.; Poonian, S.; Popoola, O.; Pora, A.; Prasad, V.; Prasad, R.; Razzaq, O.; Richardson, S.; Royal, S.; Safa, A.; Sehdev, S.; Sevenoaks, T.; Shah, D.; Sheikh, A.; Short, V.; Sidhu, B. S.; Singh, I.; Soni, Y.; Thalasselis, C.; Wilson, P.; Wingfield, D.; Wong, M.; Woodall, M. N. J.; Wooding, N.; Woods, S.; Yong, J.; Yongblah, F.; Zafar, A. Molnupiravir plus Usual Care versus Usual

Care Alone as Early Treatment for Adults with COVID-19 at Increased Risk of Adverse Outcomes (PANORAMIC): An Open-Label, Platform-Adaptive Randomised Controlled Trial. *Lancet* **2022,** *401 (10373)* 281-93. https://doi.org/10.1016/S0140-6736(22)02597-1.

(22) Szabo, B. G.; Lenart, K. S.; Petrik, B.; Gaspar, Z.; Kiss-Dala, N.; Szlavik, J.; Valyi-Nagy, I.; Lakatos, B.; Balogh, Z.; Banyai, Z.; Banyasz, E.; Budai, J.; Czel, E.; Fried, K.; Hanuska, A.; Lorinczi, C.; Nemesi, K.; Kadar, J.; Nagy, E. L.; Osvald, A.; Petrovicz, E.; Riczu, A.; Szanka, J.; Szathmary, B.; Szombati, A.; Toth, S.; Varnai, Z.; Woller, O. Favipiravir Treatment Does Not Influence Disease Progression among Adult Patients Hospitalized with Moderate-to-Severe COVID-19: A Prospective, Sequential Cohort Study from Hungary. *GeroScience* **2021**, *43* (5), 2205–2213. https://doi.org/10.1007/s11357-021-00452-9.

(23) Jimenez, D. *Paxlovid: what we know about Pfizer's Covid-19 pill*. Analysis. https://www.pharmaceutical-technology.com/analysis/paxlovid-pfizer-covid-19-pill/ (accessed 2022-09-30).

(24) National Institutes of Health. *Ritonavir-Boosted Nirmatrelvir (Paxlovid)*. NIH. https://www.covid19treatmentguidelines.nih.gov/therapies/antiviral-therapy/ritonavir-boosted-nirmatrelvir--paxlovid-/ (accessed 2022-05-09).

(25) Keretsu, S.; Bhujbal, S. P.; Cho, S. J. Rational Approach toward COVID-19 Main Protease Inhibitors via Molecular Docking, Molecular Dynamics Simulation and Free Energy Calculation. *Sci. Rep.* **2020**, *10* (1), 17716. https://doi.org/10.1038/s41598-020-74468-0.

(26) Hosseini, M.; Chen, W.; Xiao, D.; Wang, C. Computational Molecular Docking and Virtual Screening Revealed Promising SARS-CoV-2 Drugs. *Precis. Clin. Med.* **2021**, *4* (1), 1–16. https://doi.org/10.1093/PCMEDI/PBAB001.

(27) Cava, C.; Bertoli, G.; Castiglioni, I. Potential Drugs against COVID-19 Revealed by Gene Expression Profile, Molecular Docking and Molecular Dynamic Simulation. *Future Virol.* **2021**, *16* (8), 527–542. https://doi.org/10.2217/fvl-2020-0392.

(28) Lazniewski, M.; Dermawan, D.; Hidayat, S.; Muchtaridi, M.; Dawson, W. K.; Plewczynski, D. Drug Repurposing for Identification of Potential Spike Inhibitors for SARS-CoV-2 Using Molecular Docking and Molecular Dynamics Simulations. *Methods* **2022**, *203*, 498–510. https://doi.org/10.1016/j.ymeth.2022.02.004.

(29) Onyango, H.; Odhiambo, P.; Angwenyi, D.; Okoth, P. In Silico Identification of New Anti-SARS-CoV-2 Main Protease (Mpro) Molecules with Pharmacokinetic Properties from Natural Sources Using Molecular Dynamics (MD) Simulations and Hierarchical Virtual Screening. *J. Trop. Med.* **2022**, *2022*, 1–22. https://doi.org/10.1155/2022/3697498.

(30) Piplani, S.; Singh, P.; Winkler, D. A.; Petrovsky, N. Potential COVID-19 Therapies from Computational Repurposing of Drugs and Natural Products against the SARS-CoV-2 Helicase. *Int. J. Mol. Sci.* **2022**, *23* (14), 7704. https://doi.org/10.3390/ijms23147704.

(31) Sanachai, K.; Somboon, T.; Wilasluck, P.; Deetanya, P.; Wolschann, P.; Langer, T.; Lee, V. S.; Wangkanont, K.; Rungrotmongkol, T.; Hannongbua, S. Identification of Repurposing Therapeutics toward SARS-CoV-2 Main Protease by Virtual Screening. *PLoS One* **2022**, *17* (6), e0269563. https://doi.org/10.1371/journal.pone.0269563.

(32) Wouters, O. J.; McKee, M.; Luyten, J. Estimated Research and Development Investment Needed to Bring a New Medicine to Market, 2009-2018. *Jama* **2020**, *323* (9), 844–853. https://doi.org/10.1001/jama.2020.1166.

(33) Pushpakom, S.; Iorio, F.; Eyers, P. A.; Escott, K. J.; Hopper, S.; Wells, A.; Doig, A.; Guilliams, T.; Latimer, J.; McNamee, C.; Norris, A.; Sanseau, P.; Cavalla, D.; Pirmohamed, M. Drug Repurposing: Progress, Challenges and Recommendations. *Nature Reviews Drug Discovery*.

Nature Publishing Group January 12, 2018, pp 41–58. https://doi.org/10.1038/nrd.2018.168.

(34) Jain, H. A.; Agarwal, V.; Bansal, C.; Kumar, A.; Faheem, F.; Mohammed, M.-U.-R.; Murugesan, S.; Simpson, M. M.; Karpe, A. V.; Chandra, R.; MacRaild, C. A.; Styles, I. K.; Peterson, A. L.; Cooper, M. A.; Kirkpatrick, C. M. J.; Shah, R. M.; Palombo, E. A.; Trevaskis, N. L.; Creek, D. J.; Vasan, S. S. CoviRx: A User-Friendly Interface for Systematic Down-Selection of Repurposed Drug Candidates for COVID-19. *Data* **2022**, *7* (11), 164. https://doi.org/10.3390/data7110164.

(35) MacRaild, C. A.; Mohammed, M. U. R.; Faheem; Murugesan, S.; Styles, I. K.; Peterson, A. L.; Kirkpatrick, C. M. J.; Cooper, M. A.; Palombo, E. A.; Simpson, M. M.; Jain, H. A.; Agarwal, V.; McAuley, A. J.; Kumar, A.; Creek, D. J.; Trevaskis, N. L.; Vasan, S. S. Systematic Down-Selection of Repurposed Drug Candidates for COVID-19. *Int. J. Mol. Sci.* **2022**, *23* (19). https://doi.org/10.3390/ijms231911851.

(36) McAuley, A. J.; Jansen van Vuren, P.; Mohammed, M.-U.-R.; Faheem; Goldie, S.; Riddell, S.; Gödde, N. J.; Styles, I. K.; Bruce, M. P.; Chahal, S.; Keating, S.; Blasdell, K. R.; Tachedjian, M.; O'Brien, C. M.; Singanallur, N. B.; Viana, J. N.; Vashi, A. V.; Kirkpatrick, C. M.; MacRaild, C. A.; Shah, R. M.; Vincan, E.; Athan, E.; Creek, D. J.; Trevaskis, N. L.; Murugesan, S.; Kumar, A.; Vasan, S. S. Use of Human Lung Tissue Models for Screening of Drugs against SARS-CoV-2 Infection. *Viruses* **2022**, *14* (11), 2417. https://doi.org/10.3390/v14112417.

(37) Tanimoto, T. T. An Elementary Mathematical Theory of Classification and Prediction. In *Proc. IBM Internal Report*; International Business Machines Corp., 1958; pp 1–11.

(38) Kushwaha, P. P.; Singh, A. K.; Bansal, T.; Yadav, A.; Prajapati, K. S.; Shuaib, M.; Kumar, S. Identification of Natural Inhibitors Against SARS-CoV-2 Drugable Targets Using Molecular Docking, Molecular Dynamics Simulation, and MM-PBSA Approach. *Front. Cell. Infect. Microbiol.* **2021**, *11*. https://doi.org/10.3389/fcimb.2021.730288.

(39) Friesner, R. A.; Banks, J. L.; Murphy, R. B.; Halgren, T. A.; Klicic, J. J.; Mainz, D. T.; Repasky, M. P.; Knoll, E. H.; Shelley, M.; Perry, J. K.; Shaw, D. E.; Francis, P.; Shenkin, P. S. Glide: A New Approach for Rapid, Accurate Docking and Scoring. 1. Method and Assessment of Docking Accuracy. *J. Med. Chem.* **2004**, *47* (7), 1739–1749. https://doi.org/10.1021/jm0306430.

(40) Abd El-Aziz, N. M.; Eldin Awad, O. M.; Shehata, M. G.; El-Sohaimy, S. A. Inhibition of the SARS-CoV-2 RNA-Dependent RNA Polymerase by Natural Bioactive Compounds: Molecular Docking Analysis. *Egypt. J. Chem.* **2021**, *64* (4), 1989–2001. https://doi.org/10.21608/EJCHEM.2021.45739.2947.

(41) Li, D.; Luan, J.; Zhang, L. Molecular Docking of Potential SARS-CoV-2 Papain-like Protease Inhibitors. *Biochem. Biophys. Res. Commun.* **2021**, *538*, 72–79. https://doi.org/10.1016/j.bbrc.2020.11.083.

(42) Kang, S.; Yang, M.; Hong, Z.; Zhang, L.; Huang, Z.; Chen, X.; He, S.; Zhou, Z.; Zhou, Z.; Chen, Q.; Yan, Y.; Zhang, C.; Shan, H.; Chen, S. Crystal Structure of SARS-CoV-2 Nucleocapsid Protein RNA Binding Domain Reveals Potential Unique Drug Targeting Sites. *Acta Pharm. Sin. B* **2020**, *10* (7), 1228–1238. https://doi.org/10.1016/j.apsb.2020.04.009.

(43) Mulakala, C.; Viswanadhan, V. N. Could MM-GBSA Be Accurate Enough for Calculation of Absolute Protein/Ligand Binding Free Energies? *J. Mol. Graph. Model.* **2013**, *46*, 41–51. https://doi.org/10.1016/j.jmgm.2013.09.005.

(44) Shelley, J. C.; Cholleti, A.; Frye, L. L.; Greenwood, J. R.; Timlin, M. R.; Uchimaya, M. Epik: A Software Program for PKa Prediction and Protonation State Generation for Drug-like Molecules. *J. Comput. Aided. Mol. Des.* **2007**, *21* (12), 681–691.

https://doi.org/10.1007/s10822-007-9133-z.

(45) Nutt, D. R.; Smith, J. C. Molecular Dynamics Simulations of Proteins: Can the Explicit Water Model Be Varied? *J. Chem. Theory Comput.* **2007**, *3* (4), 1550–1560. https://doi.org/10.1021/ct700053u.

(46) Lu, C.; Wu, C.; Ghoreishi, D.; Chen, W.; Wang, L.; Damm, W.; Ross, G. A.; Dahlgren, M. K.; Russell, E.; Von Bargen, C. D.; Abel, R.; Friesner, R. A.; Harder, E. D. OPLS4: Improving Force Field Accuracy on Challenging Regimes of Chemical Space. *J. Chem. Theory Comput.* **2021**, *17* (7), 4291–4300. https://doi.org/10.1021/acs.jctc.1c00302.

(47) Hevener, K. E.; Zhao, W.; Ball, D. M.; Babaoglu, K.; Qi, J.; White, S. W.; Lee, R. E. Validation of Molecular Docking Programs for Virtual Screening against Dihydropteroate Synthase. *J. Chem. Inf. Model.* **2009**, *49* (2), 444–460. https://doi.org/10.1021/ci800293n.

(48) Ribeiro, E.; Araújo, D.; Pereira, M.; Lopes, B.; Sousa, P.; Sousa, A. C.; Coelho, A.; Rêma, A.; Alvites, R.; Faria, F.; Oliveira, C.; Porto, B.; Maurício, A. C.; Amorim, I.; Vale, N. Repurposing Benztropine, Natamycin, and Nitazoxanide Using Drug Combination and Characterization of Gastric Cancer Cell Lines. *Biomedicines* **2023**, *11* (3), 799. https://doi.org/10.3390/biomedicines11030799.

(49) Milani, M.; Donalisio, M.; Bonotto, R. M.; Schneider, E.; Arduino, I.; Boni, F.; Lembo, D.; Marcello, A.; Mastrangelo, E. Combined in Silico and in Vitro Approaches Identified the Antipsychotic Drug Lurasidone and the Antiviral Drug Elbasvir as SARS-CoV2 and HCoV-OC43 Inhibitors. *Antiviral Res.* **2021**, *189*, 105055. https://doi.org/10.1016/j.antiviral.2021.105055.

(50) Avram, S.; Wilson, T. B.; Curpan, R.; Halip, L.; Borota, A.; Bora, A.; Bologa, C. G.; Holmes, J.; Knockel, J.; Yang, J. J.; Oprea, T. I. DrugCentral 2023 Extends Human Clinical Data and Integrates Veterinary Drugs. *Nucleic Acids Res.* **2023**, *51* (D1), D1276–D1287. https://doi.org/10.1093/nar/gkac1085.

(51) Whittle, B. J.; Silverstein, A. M.; Mottola, D. M.; Clapp, L. H. Binding and Activity of the Prostacyclin Receptor (IP) Agonists, Treprostinil and Iloprost, at Human Prostanoid Receptors: Treprostinil Is a Potent DP1 and EP2 Agonist. *Biochem. Pharmacol.* **2012**, *84* (1), 68–75. https://doi.org/10.1016/j.bcp.2012.03.012.

(52) Jansen van Vuren, P.; McAuley, A. J.; Kuiper, M. J.; Singanallur, N. B.; Bruce, M. P.; Riddell, S.; Goldie, S.; Mangalaganesh, S.; Chahal, S.; Drew, T. W.; Blasdell, K. R.; Tachedjian, M.; Caly, L.; Druce, J. D.; Ahmed, S.; Khan, M. S.; Malladi, S. K.; Singh, R.; Pandey, S.; Varadarajan, R.; Vasan, S. S. Highly Thermotolerant SARS-CoV-2 Vaccine Elicits Neutralising Antibodies against Delta and Omicron in Mice. *Viruses* **2022**, *14* (4), 800. https://doi.org/10.3390/v14040800.

(53) Ahmed, S. F.; Quadeer, A. A.; McKay, M. R. Preliminary Identification of Potential Vaccine Targets for the COVID-19 Coronavirus (SARS-CoV-2) Based on SARS-CoV Immunological Studies. *Viruses* **2020**, *12* (3), 254. https://doi.org/10.3390/v12030254.

(54) Fu, Y.; Cheng, Y.; Wu, Y. Understanding SARS-CoV-2-Mediated Inflammatory Responses: From Mechanisms to Potential Therapeutic Tools. *Virol. Sin.* **2020**, *35* (3), 266–271. https://doi.org/10.1007/s12250-020-00207-4.

(55) Jawad, B.; Adhikari, P.; Podgornik, R.; Ching, W.-Y. Key Interacting Residues between RBD of SARS-CoV-2 and ACE2 Receptor: Combination of Molecular Dynamics Simulation and Density Functional Calculation. *J. Chem. Inf. Model.* **2021**, *61* (9), 4425–4441. https://doi.org/10.1021/acs.jcim.1c00560.

(56) Tatar, G.; Ozyurt, E.; Turhan, K. Computational Drug Repurposing Study of the RNA Binding

Domain of SARS-CoV-2 Nucleocapsid Protein with Antiviral Agents. *Biotechnol. Prog.* **2021**, *37*:e3110. https://doi.org/10.1002/btpr.3110.

(57) Báez-Santos, Y. M.; St. John, S. E.; Mesecar, A. D. The SARS-Coronavirus Papain-like Protease: Structure, Function and Inhibition by Designed Antiviral Compounds. *Antiviral Res.* **2015**, *115*, 21–38. https://doi.org/10.1016/j.antiviral.2014.12.015.

(58) Ahmad, B.; Batool, M.; Ain, Q. ul; Kim, M. S.; Choi, S. Exploring the Binding Mechanism of PF-07321332 SARS-CoV-2 Protease Inhibitor through Molecular Dynamics and Binding Free Energy Simulations. *Int. J. Mol. Sci.* **2021**, *22* (17), 9124. https://doi.org/10.3390/ijms22179124.

(59) Zhang, L.; Lin, D.; Sun, X.; Curth, U.; Drosten, C.; Sauerhering, L.; Becker, S.; Rox, K.; Hilgenfeld, R. Crystal Structure of SARS-CoV-2 Main Protease Provides a Basis for Design of Improved α-Ketoamide Inhibitors. *Science*. **2020**, *368* (6489), 409–412. https://doi.org/10.1126/science.abb3405.

(60) Aftab, S. O.; Ghouri, M. Z.; Masood, M. U.; Haider, Z.; Khan, Z.; Ahmad, A.; Munawar, N. Analysis of SARS-CoV-2 RNA-Dependent RNA Polymerase as a Potential Therapeutic Drug Target Using a Computational Approach. *J. Transl. Med.* **2020**, *18* (1), 275. https://doi.org/10.1186/s12967-020-02439-0.

(61) Adedeji, A. O.; Marchand, B.; te Velthuis, A. J. W.; Snijder, E. J.; Weiss, S.; Eoff, R. L.; Singh, K.; Sarafianos, S. G. Mechanism of Nucleic Acid Unwinding by SARS-CoV Helicase. *PLoS One* **2012**, *7* (5), e36521. https://doi.org/10.1371/journal.pone.0036521.

(62) Pitsillou, E.; Liang, J.; Hung, A.; Karagiannis, T. C. The SARS-CoV-2 Helicase as a Target for Antiviral Therapy: Identification of Potential Small Molecule Inhibitors by in Silico Modelling. *J. Mol. Graph. Model.* **2022**, *114*, 108193. https://doi.org/10.1016/j.jmgm.2022.108193.

(63) Tahir, M. Coronavirus Genomic Nsp14-ExoN, Structure, Role, Mechanism, and Potential Application as a Drug Target. *J. Med. Virol.* **2021**, *93* (7), 4258–4264. https://doi.org/10.1002/jmv.27009.

(64) Ogando, N. S.; Zevenhoven-Dobbe, J. C.; van der Meer, Y.; Bredenbeek, P. J.; Posthuma, C. C.; Snijder, E. J. The Enzymatic Activity of the Nsp14 Exoribonuclease Is Critical for Replication of MERS-CoV and SARS-CoV-2. *J. Virol.* **2020**, *94* (23). https://doi.org/10.1128/JVI.01246-20.

(65) Ma, Y.; Wu, L.; Shaw, N.; Gao, Y.; Wang, J.; Sun, Y.; Lou, Z.; Yan, L.; Zhang, R.; Rao, Z. Structural Basis and Functional Analysis of the SARS Coronavirus Nsp14–Nsp10 Complex. *Proc. Natl. Acad. Sci.* **2015**, *112* (30), 9436–9441. https://doi.org/10.1073/pnas.1508686112.

(66) Mulia, E. P. B.; Luke, K. Inhaled Prostacyclin Analogues in COVID-19 Associated Acute Respiratory Distress Syndrome: Scientific Rationale. *Egypt. Hear. J.* **2021**, *73* (1), 82. https://doi.org/10.1186/s43044-021-00208-y.

(67) Nasrullah, A.; Virk, S.; Shah, A.; Jacobs, M.; Hamza, A.; Sheikh, A. B.; Javed, A.; Butt, M. A.; Sangli, S. Acute Respiratory Distress Syndrome and the Use of Inhaled Pulmonary Vasodilators in the COVID-19 Era: A Narrative Review. *Life* **2022**, *12* (11), 1766. https://doi.org/10.3390/life12111766.

(68) Rajpal, S. *Inpatient use of inhaled pulmonary vasodilator therapy in patients infected with COVID-19*. American college of cardiology. https://www.acc.org/latest-in-cardiology/articles/2020/05/13/08/55/inpatient-use-of-inhaled-pulmonary-vasodilator-therapy-in-patients-infected-with-covid-19 (accessed 2023-06-05).

(69) Degli Esposti, L.; Perrone, V.; Sangiorgi, D.; Andretta, M.; Bartolini, F.; Cavaliere, A.; Ciaccia, A.; Dell'orco, S.; Grego, S.; Salzano, S.; Ubertazzo, L.; Vercellone, A.; Gatti, D.; Fassio, A.;

Viapiana, O.; Rossini, M.; Adami, G. The Use of Oral <scp>Amino-Bisphosphonates</Scp> and Coronavirus Disease 2019 (COVID-19) Outcomes. *J. Bone Miner. Res.* **2021**, *36* (11), 2177–2183. https://doi.org/10.1002/jbmr.4419.

(70) Thompson, J.; Wang, Y.; Dreischulte, T.; Barreiro, O.; Gonzalez, R. J.; Hanč, P.; Matysiak, C.; Neely, H. R.; Rottenkolber, M.; Haskell, T.; Endres, S.; von Andrian, U. H. Association between Bisphosphonate Use and COVID-19 Related Outcomes: A Retrospective Cohort Study. *medRxiv* **2022**, 2022.06.14.22276397. https://doi.org/10.1101/2022.06.14.22276397.

(71) Murugan, N. A.; Kumar, S.; Jeyakanthan, J.; Srivastava, V. Searching for Target-Specific and Multi-Targeting Organics for Covid-19 in the Drugbank Database with a Double Scoring Approach. *Sci. Rep.* **2020**, *10*, 19125. https://doi.org/10.1038/s41598-020-75762-7.

(72) Staten, M. *New COVID-19 treatment being explored at TTUHSC El Paso*. https://www.krwg.org/regional/2022-01-19/new-covid-19-treatment-being-explored-at-ttuhsc-el-paso (accessed 2023-06-06).

(73) Michelson, E. *Cromolyn sodium for treatment of COVID-19 pneumonia*. ClinicalTrials.gov. https://clinicaltrials.gov/ct2/show/NCT05077917.

(74) Miranda-Quintana, R. A.; Bajusz, D.; Rácz, A.; Héberger, K. Extended Similarity Indices: The Benefits of Comparing More than Two Objects Simultaneously. Part 1: Theory and Characteristics†. *J. Cheminform.* **2021**, *13*, 32. https://doi.org/10.1186/s13321-021-00505-3.

(75) Miranda-Quintana, R. A.; Rácz, A.; Bajusz, D.; Héberger, K. Extended Similarity Indices: The Benefits of Comparing More than Two Objects Simultaneously. Part 2: Speed, Consistency, Diversity Selection. *J. Cheminform.* **2021**, *13*, 33. https://doi.org/10.1186/s13321-021-00504-4.